THE GEOLOGICAL SOCIETY OF AMERICA®

Along-strike variations in sediment provenance within the Nanaimo basin reveal mechanisms of forearc basin sediment influx events

Daniel S. Coutts, William A. Matthews, Rebecca G. Englert, Morgan D. Brooks, Marie-Pier Boivin, and Stephen M. Hubbard
DEPARTMENT OF GEOSCIENCE, UNIVERSITY OF CALGARY, 2500 UNIVERSITY DRIVE NW, CALGARY, ALBERTA, CANADA T2N 1N4

ABTRACT

The along-strike variability in sediment provenance within the Nanaimo basin is important for understanding the tectonic evolution of North America's Late Cretaceous Pacific margin, providing context for paleogeographic reconstructions. Here, we provide 35 point-counted sandstone samples and 22 new detrital zircon samples from the Nanaimo basin. These new detrital zircon samples compose a portion of a basin-wide data set (N = 49, n = 10,942) that is leveraged to discern spatio-temporal changes in sediment provenance. Provenance data demonstrates that the majority of Nanaimo basin strata were sourced from regions within and east of the Coast Mountains Batholith, while only the southernmost Nanaimo basin, exposed in the San Juan Islands, was supplied sediment from the North Cascade thrust system. Additionally, near-identical age modes and synchronous changes in detrital zircon facies are used to hypothesize a correlation between the Nanaimo Group and the protolith of the Swakane Gneiss. These observations, along with previously identified events in the Cordillera, are used to define two basin-wide events that affected the Nanaimo basin: the first at 84 Ma and the second at 72 Ma. The first event is correlated to the onset of Kula-Farallon spreading, which affected basin subsidence, introduced Proterozoic detrital zircon to the central and southern Nanaimo basin, and uplifted the North Cascade thrust system. The second basin-wide event, which is speculated to have been driven by increased rates of subduction and obliquity, resulted in localized high-flux events in the arc, increased exhumation of the Cascade Crystalline Core, underplating of the Swakane Gneiss, and coarse-grained sedimentation across the basin. The data presented here provides added context for the evolution of the basin and provides insight into the protracted geodynamics of forearc basins undergoing oblique subduction.

LITHOSPHERE; v. 12; no. 1; p. 180–197; GSA Data Repository Item 2020133 | Published online 12 February 2020 https://doi.org/10.1130/L1138.1

INTRODUCTION

Detrital minerals preserved in sedimentary basins reflect tectonic processes that deform, uplift, or bury sediment sources in the hinterland (Pettijohn et al., 1972; Ingersoll, 1978; Dickinson, 1982; Fedo et al., 2003; Whitchurch et al., 2011; Sharman et al., 2015; Orme and Laskowski, 2016; Horton, 2018). As such, the tectonic evolution of orogenic belts is often deciphered from their eroded, detrital components preserved in sedimentary basins (Dickinson, 1982; Fedo et al., 2003; Gehrels et al., 2008). However, the interpretation of tectonic events from basin stratigraphy is complicated by diachronous, along-strike variations that are common in convergent orogens (e.g., Kley et al., 1999; Yin, 2006; Horton, 2018). Along-strike variability can be controlled by several factors, including: changes in magmatic tempo (e.g., Paterson and Ducea, 2015; Cecil et al., 2018), style of deformation and uplift (e.g., Whitchurch et al., 2011; Fitz-Díaz et al., 2018), or arc/basement lithology (e.g., Sundell et al., 2018). Thus, the use of spatially and temporally limited provenance data sets to examine the evolution of hinterland source areas may lead to an incomplete understanding of hinterland evolution or the extent of tectonic mechanisms that drive sedimentation (e.g., Yin, 2006; Cecil et al., 2018; Horton, 2018). Large, basin-scale data sets paired with information regarding hinterland evolution (e.g., exhumation rates, radiometric ages bracketing deformation) reveal intimate details of orogenic processes and their effects on basin sedimentation (e.g., Whitchurch et al., 2011; Saylor et al., 2012; Sundell et al., 2018).

The Nanaimo basin of British Columbia, Canada, is one of many sedimentary basins that sequestered sediments along the Pacific margin of the North American Cordillera throughout Late Cretaceous to Early Paleogene time. These basins preserve a record of the final building stages of the Cordillera (Dickinson, 1976; Surpless et al., 2014; Busby, 2004), including periods of hinterland deformation (Mustard, 1994; Brown, 2012; Sharman et al., 2015), high-flux volcanism (Kimbrough et al., 2001; Englert et al., 2018), changes in subduction angles (Moxon and Graham, 1987; Dickinson et al., 1983; Fitz-Díaz et al., 2018), and differential uplift rates (Saleeby, 2003; Busby, 2004). Therefore, provenance analysis of basin fill deposits, such as the Nanaimo Group, can aid in understanding the protracted diachroneity, spatial extent, and interaction of these processes within the framework of the Late Cretaceous to Paleogene evolution of the Cordillera.

The Late Cretaceous to Paleocene Nanaimo basin is preserved adjacent to many of its sediment source regions (Mustard et al., 1995; Katnick and Mustard, 2003; Brown, 2012; Matthews et al., 2017), including: (1) the Coast mountains batholith, an eroded magmatic arc with along-strike variations in magmatic tempo (Friedman and Armstrong, 1995; Gehrels et al., 2008; Cecil et al., 2018); (2) the Wrangellia terrane, which forms

Daniel S. Coutts http://orcid.org/0000-0002-2345-2865

the basement of the basin (Greene et al., 2010); and (3) the North Cascade thrust system, a fold-and-thrust belt composed of lithologically diverse terranes located at the southern margin of the basin (e.g., Brandon et al., 1988; Brown and Gehrels, 2007; Brown et al., 2010; Brown, 2012; Sauer et al., 2017). Although proximal sediment sources are established, interpretations of distal sediment sources are contentious, and have been used to interpret the Late Cretaceous paleolatitude of the basin (Matthews et al., 2017, and references therein). Additionally, the presence, relative sediment contributions, and structural evolution of the different source areas have been used to account for the primary mechanism of basin subsidence. Thus, interpretations of the tectonic setting include forearc (Muller and Jeletzky, 1970; England, 1990; Matthews et al., 2017; Englert et al., 2018; Kent et al., 2019), foreland (Brandon et al., 1988; Mustard, 1994), and strike-slip basin (Pacht, 1984).

Only recently have large-*n* laser ablation–inductively coupled plasma–mass spectrometry (LA-ICP-MS) detrital zircon techniques been used to unravel contentious ideas about the origin of Nanaimo basin strata (Matthews et al., 2017; Englert et al., 2018; Huang et al., 2019; Kent et al., 2019). However, a basin-wide investigation of spatial and temporal changes in provenance has the potential to answer numerous outstanding questions regarding sediment transfer along the Pacific margin of North America. For example, the relative supply from regional sources (e.g., North Cascade thrust system and Coast Mountains Batholith) may help determine basin forming processes. Additionally, the protracted record of the Nanaimo Group (Turonian to Danian) allows for a spatio-temporal analysis of the interplay between subduction, magmatism, and sedimentation in forearc regions along the 160-km-long outcrop belt.

In this study, we use an integrated provenance data set including sandstone petrography and data from 22 new detrital zircon samples (n = 4534) to deduce provenance variability along a 160-km-long depositional-strike-oriented transect of the Nanaimo basin. These new data, along with existing data from Matthews et al. (2017) and Englert et al. (2018), compose a basin-wide detrital zircon database (N = 49, n = 10,942) that provide insight into the along-strike influence of sediment source areas and hinterland/subduction zone processes during basin filling. In doing so, we demonstrate: (1) the sequential emplacement of the terranes that compose the North Cascade Thrust system and their recycling into a limited portion of the Nanaimo basin; (2) the protolith of the Swakane Biotite-Gneiss was derived from source terranes similar to the Nanaimo Group; and (3) a correlation of changes in the Kula plate subduction vectors with changes in both basin sedimentation patterns and hinterland evolution. These results provide strong constraints on the drivers of Nanaimo Group sedimentation and tectonic processes during a contentious period in the geologic history of the northern Cordillera, which can be applied to understand the large-scale geodynamics of forearc systems.

GEOLOGIC SETTING OF THE NANAIMO BASIN

The North American Cordillera is composed of numerous allochthonous fault-bounded terranes that accreted to the western margin of Laurentia as well as volcanic arcs, which, in some cases, stitch terranes together (Monger et al., 1982, and many others). Jurassic to Eocene subduction beneath western North America formed a volcanic arc that spanned from Washington, USA, to Yukon, Canada, the eroded remnant of which is known as the Coast Mountains Batholith (Monger et al., 1982). The Coast Mountains Batholith composes a minor portion of the basement of the Late Cretaceous to Paleogene Nanaimo basin (Mustard, 1994). Plutonism in the Coast Mountains Batholith contains both orogen-wide (ca. 150 Ma) and more localized high-flux events (e.g., Friedman and Armstrong 1995; Gehrels et al., 2009; Beranek et al., 2017; Cecil et al., 2018). Of relevance to the Nanaimo basin are: (1) the southern Coast Mountains Batholith, which ranges in age between 160 and 40 Ma and is associated with high-flux events that occurred between 85–70 Ma and 61–48 Ma (Cecil et al., 2018); (2) the Vancouver Coast Mountains Batholith, which ranges in age between 180 and 60 Ma and is associated with high flux events that occurred between 105–90 Ma and 70–60 Ma (Friedman and Armstrong, 1995) (Fig. 1); and (3) the Cascade Crystalline Core (CCC), which is the most deeply exhumed portion of the Coast Mountains Batholith (Tabor et al., 1987) (Fig. 1), composed of metamorphosed plutonic rocks, volcanic rocks, and forearc sediments that were incorporated into the arc at mid-to-deep-crustal depths (e.g., Swakane Biotite-Gneiss) (Tabor et al., 1987; Matzel et al., 2004; Ducea and Chapman, 2018; Sauer et al., 2017, 2018). Magmatic activity in the CCC spans 96–45 Ma, and high flux events occurred between 96–89 Ma and 78–71 Ma (Miller et al., 2009). Due to changes in subduction and crustal thickening in the Coast Mountains Batholith, magmatism migrated eastward through time and no plutonic activity occurred within 100 km of the modern coastline post–70 Ma (Cecil et al., 2018).

The Insular Superterrane, composed of Alexander and Wrangellia terranes, accreted to the western margin of the Coast Mountains Batholith and already-accreted Intermontane Superterrane during the Late Jurassic to Early Cretaceous. The Wrangellia terrane constitutes the majority of the basement of the Nanaimo basin, composed of >10 km of igneous rocks and lesser sedimentary strata, which ranges in age from Devonian to Jurassic (Yorath et al., 1999; Greene et al., 2010). The timing and latitude of Insular Superterrane accretion to North America is debated. Some suggest accretion occurred during or prior to the Early Jurassic (e.g., Monger et al., 1982; Monger and Gibson, 2019), while others suggest accretion took place during the Early Cretaceous (e.g., Sigloch and Mihalynuk, 2017).

After the collision of the Insular Superterrane, Coast Mountains Batholith magmatism was largely driven by subduction of the Farallon plate. This subduction continued, roughly normal to the margin of North America, until the Farallon plate rifted into the Kula and Farallon plates. Magnetic lineations indicate that seafloor spreading at the Pacific-Kula ridge was ongoing by 79 Ma (Atwater, 1989; Seton et al., 2012), although rifting as early as 85 Ma has been estimated (Woods and Davies, 1982; Engebretson et al., 1985). Rifting reoriented the subduction vector from roughly normal to the North American margin to highly oblique (Woods and Davies, 1982; Engebretson et al., 1985; Doubrovine and Tarduno, 2008). Oblique subduction of the Kula Plate drove the accretion of additional terranes (e.g., Eddy et al., 2017), structural evolution of the Nanaimo basin (e.g., Kent et al., 2019), and changes in stress regime within the Cordillera (e.g., Umhoefer and Miller, 1996).

The southern margin of the Nanaimo basin is defined by the North Cascade thrust system (NCTS). The NCTS is composed of multiple fault-bounded terranes, exposed between the west side of the Fraser–Straight Creek fault zone and Haro Strait (Fig. 1B). Terranes incorporated in the NCTS vary in age from early Paleozoic to Early Cretaceous (Vance 1975; Garver, 1988; Rubin et al., 1990) and are lithologically (Vance, 1975; Brandon et al., 1988; Garver, 1988; Schermer et al., 2018), geochronologically (Brown and Gehrels, 2007; Brown et al., 2010; Brown, 2012; Sauer et al., 2017; Schermer et al., 2018), and thermochronologically diverse (Johnson et al., 1986; Brandon et al., 1988; Brown et al., 2005). Small sedimentary successions within the NCTS (e.g., exposures on Barnes Island and Blakey Island) have been correlated to the Nanaimo Group based on lithostratigraphic descriptions (Vance, 1975) and detrital zircon age distributions (Brown, 2012) (Fig. 1). The thrust nappes within the NCTS include the Chilliwack nappe, Orcas nappe, Shuskan nappe, and

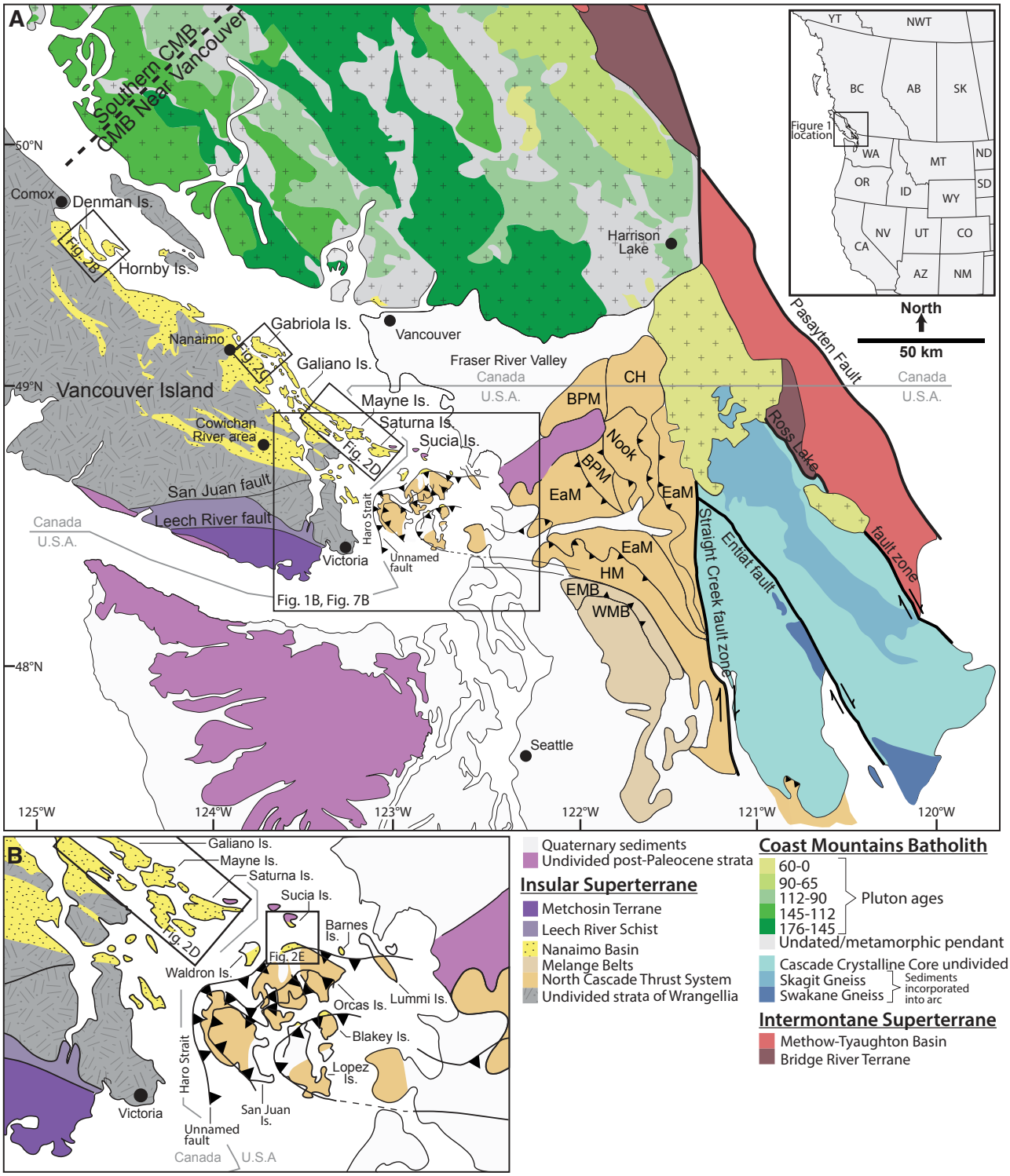

Figure 1. (A) Simplified geologic map of southern British Columbia, Canada, and northern Washington, USA, demonstrating the tectonic context of the Nanaimo basin. (B) Detailed portion of the larger map focused on the southern Gulf Islands and San Juan Islands. Map abbreviations: BPM—Bell Pass mélange; CH—Chilliwack Terrane; CMB—Coast Mountains Batholith; EaM—Easton Metamorphic complex; EMB—Eastern mélange belt; HM—Haystack mélange; Nook—Nooksack Terrane; WMB—Western mélange belt. Map data is adapted from Fairchild and Cowan (1982), Friedman and Armstrong (1995), Surpless et al. (2014), Brown (2012), Eddy et al. (2017), Sauer et al. (2017), Cecil et al. (2018), and Sauer et al. (2018).

Haystack nappe, listed in order of ascending structural level (Brandon et al., 1988) and decreasing relative emplacement age (Brown, 2012). Detrital zircon maximum depositional ages and provenance relationships were used by Brown (2012) to suggest that the terranes exposed in the San Juan Islands were juxtaposed and uplifted between ca. 93 and post–87 Ma, and subsequently recycled into the Nanaimo basin during deposition of the Nanaimo Group.

The Nanaimo basin, along with many of the geologic elements that compose the tectonic framework surrounding the Nanaimo basin (i.e., Coast Mountains Batholith, NCTS, and CCC) are hypothesized to have been located between 1000 and 3000 km south of their current location during the Late Cretaceous (Umhoefer, 1987; Cowan et al., 1997). This hypothesis, known as the Baja-BC hypothesis, was originally established through the use of paleomagnetic methods (e.g., Cowan et al., 1997; Enkin et al., 2001); however, it has since been tested using structural field relationships (e.g., Wyld et al., 2006), biostratigraphic correlations (e.g., Carter and Haggart, 2006), and U-Pb detrital zircon methods (e.g., Matthews et al., 2017), with no clear result. As translation is hypothesized to have occurred during the Late Cretaceous (e.g., Cowan et al., 1997; Enkin et al., 2001), the Nanaimo basin has been a focus of this debate (Matthews et al., 2017, and references therein).

FORMATION OF THE NANAIMO BASIN AND DEPOSITION OF THE NANAIMO GROUP

The Nanaimo basin formed atop the Wrangellia terrane during the early Late Cretaceous (i.e., Turonian) between the Coast Mountains Batholith to the east and the subducting Kula-Farallon Plate to the west (Muller and Jeletzky, 1970; Haggart et al., 2005). Although the Nanaimo basin is in a forearc position, Cretaceous-age thrust sheets within the Coast Mountains Batholith (Rusmore and Woodsworth, 1994; Journeay and Friedman, 1993; Umhoefer and Miller, 1996) and NCTS (Brandon et al., 1988) are commonly thought to have supplied sediment to the basin throughout its evolution (Pacht, 1984; Mustard, 1994; Brown, 2012) (Fig. 1). As such, the Nanaimo basin has been interpreted as a forearc (e.g., Dickinson, 1976; Muller and Jeletzky, 1970; England, 1990; Matthews et al., 2017; Englert et al., 2018; Kent et al., 2019) or a foreland basin (e.g., Brandon et al., 1988; Mustard, 1994; Katnick and Mustard, 2003; Brown, 2012).

The Nanaimo Group is divided into lower and upper intervals based on regional lithostratigraphic correlations and interpreted depositional settings (Clapp, 1914; Muller and Jeletzky, 1970; Mustard, 1994) (Fig. 2A). The lower Nanaimo Group is composed of both non-marine and marginal-marine strata (Mustard, 1994; Jones et al., 2018; Huang et al., 2019; Kent

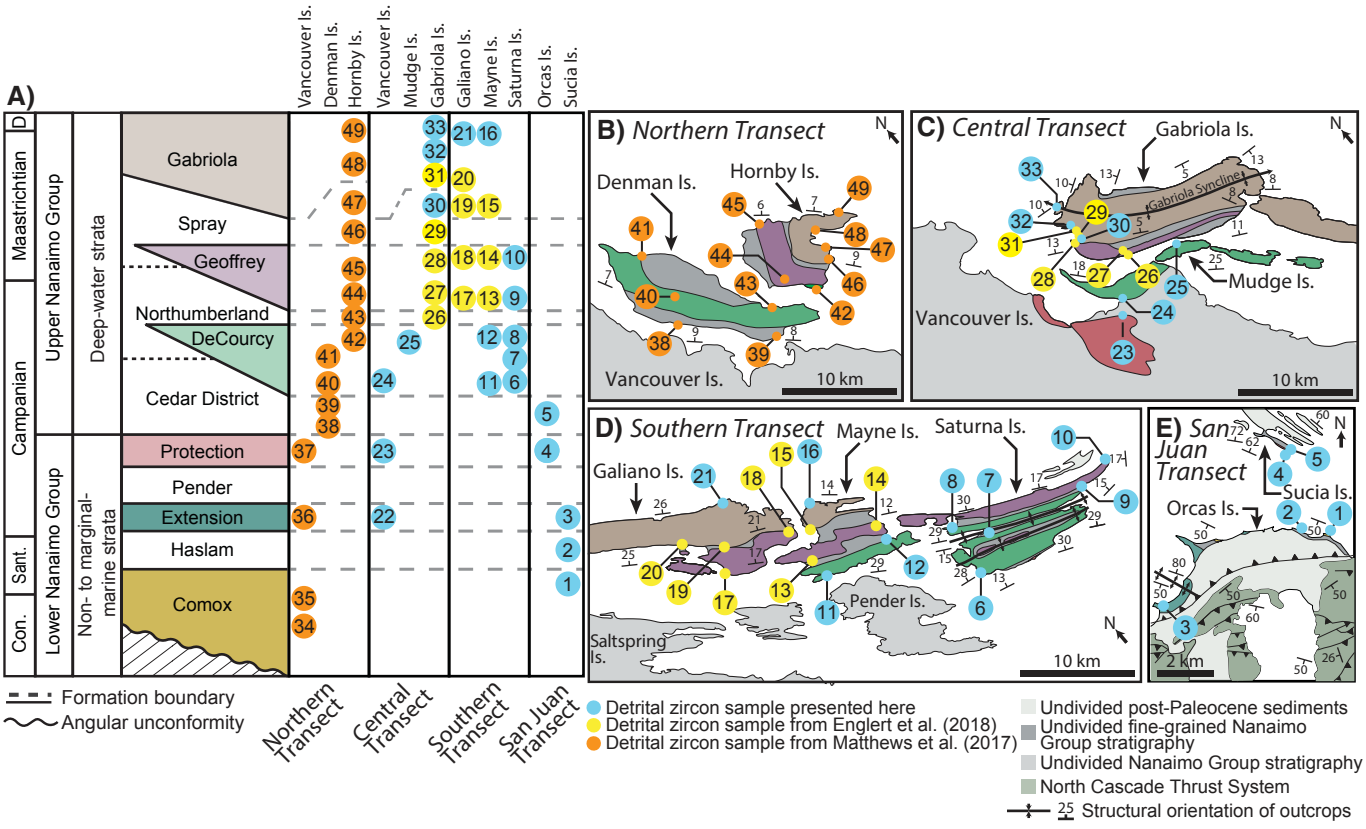

Figure 2. Stratigraphic nomenclature of the Nanaimo Group along with sample locations. (A) Stratigraphic chart of the Nanaimo Group modified from Matthews et al. (2017) using the unified formation names of Muller and Jeletzky (1970). Detrital zircon samples of the four transects (labeled at the bottom of chart) are numbered and are organized according to sampled formation, as well as island (top of chart). Sample numbers are colored by original publication. Con.—Coniacian; Sant.—Santonian; D—Danian. (B) Simplified geologic map and sample locations from the northern Gulf Islands transect that includes strata on Vancouver, Hornby, and Denman islands. Sample locations for samples 34–37 lie outside of the map area and UTM coordinates are presented in File DR2 (see footnote 1). (C) Simplified geologic map with sample locations from the central Gulf Islands transect that includes strata on Vancouver, Mudge, and Gabriola islands. UTM coordinates for sample 22 are presented in File DR2. (D) Simplified geologic map with sample locations from the southern Gulf Islands transect that includes strata on Saturna, Mayne, and Galiano islands. (E) Simplified geologic map and sample locations of the San Juan Islands transect that includes strata on Orcas and Sucia islands.

et al., 2019) (Fig. 2A). The upper Nanaimo Group is composed of deep-water depositional system deposits (e.g., submarine canyon or channel deposits) that record sediment routing during the Late Cretaceous to Paleogene (Fig. 2A) (England and Hiscott, 1992; Rowe et al., 2002; Bain and Hubbard, 2016; Englert et al., 2018, 2019).

Provenance of the Nanaimo Group

The sediment provenance of the Nanaimo Group has been interpreted based on sandstone and conglomerate clast petrology (Pacht, 1984; Mustard, 1994; Katnick and Mustard, 2003; Brown, 2012), and U-Pb detrital zircon age distributions (Mustard et al., 1995; Housen and Beck, 1999; Mahoney et al., 1999; Brown, 2012; Matthews et al., 2017; Englert et al., 2018; Huang et al., 2019). The adjacent Coast Mountains Batholith is considered the dominant sediment source for the basin, as evidenced by abundant plutonic detritus, volcanic lithic fragments in the Nanaimo Group sandstones, and Mesozoic detrital zircon ages (Mustard, 1994; Matthews et al., 2017; Fig. 1). The rocks of the NCTS are thought to be a local source of detritus to the central and southern portions of the basin during the deposition of the lower Nanaimo Group providing chert and metamorphic clasts (Pacht, 1984; Brandon et al., 1988), as well as Precambrian zircon (e.g., Mustard et al., 1995; Brown, 2012).

Previous detrital zircon work has identified two detrital zircon facies (cf. LaMaskin, 2012) in the Nanaimo basin, each composed of various age distributions: (1) dominantly Mesozoic ages (150 and 90 Ma age modes); and (2) both Mesozoic (84 and 77 Ma age modes) and Proterozoic ages (1700 and 1380 Ma age modes) (Mustard et al., 1995; Matthews et al., 2017). Mesozoic ages are interpreted to be sourced from the Coast Mountains Batholith (e.g., Mustard et al., 1995; Matthews et al., 2017), whereas source areas spanning from northern Idaho to southern California have been proposed for the Proterozoic zircons, including the Belt-Purcell basin (Mustard et al., 1995; Mahoney et al., 1999; Dumitru et al., 2016), Yavapai-Mazatzal basement (Housen and Beck, 1999), the NCTS (Brown, 2012), and the Mojave-Sonoran region (Matthews et al., 2017). Matthews et al. (2017) dated a transect of detrital zircon samples through the northern Nanaimo basin (N = 16, n = 3964; Fig. 2B) and demonstrated that Proterozoic grains were introduced to the basin during deposition of the Geoffrey Formation, ca. 72–70 Ma. The introduction of these grains has been interpreted as the eastward expansion of river drainages through the Coast Mountains Batholith into sediment source areas east of the arc (Matthews et al., 2017; Englert et al., 2018).

METHODS

Sandstone Petrology and Point Counting Methods

Thirty-five thin sections were cut from sandstones that were used for detrital zircon analysis. Thin sections were stained for potassium feldspar and a compositional and textural analysis was performed using a Nikon Eclipse LV100 petrographic microscope paired with a digital stepping stage. Petrog™ software was used to aid in the tabulation of 400 points per sample. Framework clasts were classified as quartz (chert, monocrystalline, or polycrystalline), feldspar (plagioclase or potassium-feldspar), biotite, muscovite, amphibole, hornblende, clinopyroxene, epidote, and rock fragments (volcanic, plutonic, metamorphic, or sedimentary). Standard Q-F-R (Pettijohn et al., 1972) and Q_m-F-L_t (Dickinson et al., 1983) ternary diagrams were used to characterize sandstone composition and broadly interpret tectonic setting. Complete petrologic data is available in GSA Data Repository File DR1[1].

U-Pb Detrital Zircon Geochronology Methods

Twenty-two new detrital zircon samples from the southern Nanaimo basin were analyzed (Fig. 2). These samples were added to the existing samples of Matthews et al. (2017) and Englert et al. (2018) to compose four transects referred to herein as: (1) the northern Gulf Islands transect, collected in the Comox area (Comox, Extension, and Protection formations), on Denman Island (Cedar District, DeCourcy, and Northumberland formations), and on Hornby Island (DeCourcy, Geoffrey, Spray, and Gabriola formations); (2) the central Gulf Island transect, collected in the Nanaimo area (Extension, Protection, and DeCourcy formations), on Mudge Island (DeCourcy Formation), and Gabriola Island (Northumberland through Gabriola formations) (Figs. 2A and 2B); (3) the southern Gulf Islands transect, collected across Galiano Island (Geoffrey and Gabriola formations), Mayne Island (DeCourcy, Geoffrey, and Gabriola formations), and Saturna Island (DeCourcy, and Geoffrey formations) (Figs. 2A and 2C); and (4) the San Juan Islands transect, collected across Orcas Island (Comox, Haslam, and Extension formations) and Sucia Island (Protection and Cedar District formations) (Figs. 2 and 2D).

For each sample, detrital zircon grains were isolated using standard mineral separation methods (Fedo et al., 2003). Three hundred grains were measured for each sample using LA-ICP-MS to obtain U/Pb ratios and dates following the procedure of Matthews and Guest (2017). The method used to calculate date uncertainties is in alignment with community derived best-practices outlined in Horstwood et al. (2016) but is slightly modified from Matthews and Guest (2017) (see Data Repository for details). In this study $^{206}Pb/^{238}U$ dates were used for grains yielding dates <1000 Ma whereas $^{207}Pb/^{206}Pb$ dates were used for grains yielding dates >1000 Ma. Complete isotopic data for the analyzed samples are available in Data Repository File DR2.

The toolset detritalPy (Sharman et al., 2018) was used to create probability density functions (PDFs) for individual samples and groups of samples presented here, as well as for additional published data sets (e.g., Brown, 2012; Sauer et al., 2018). Previously published data were filtered and presented in the same manner as new data reported here to enable comparisons. Reported systematic uncertainties were used to calculate total uncertainties for individual dates (S_{total}). When systematic uncertainties were not reported, 1.5% (2σ) was added in quadrature to reported $^{238}U/^{206}Pb$ ratio uncertainties and 1% (2σ) was added in quadrature to reported $^{207}Pb/^{206}Pb$ ratio uncertainties.

Calculation of Detrital Zircon Maximum Depositional Ages

Maximum depositional ages of the 22 detrital zircon samples presented here, along with 27 samples presented in Matthews et al. (2017) and Englert et al. (2018), were calculated with Isoplot (v. 4.15; Ludwig, 2012) using the youngest grain cluster that overlaps at 2σ uncertainty method (YGC 2σ) (Dickinson and Gehrels, 2009). The YGC 2σ method is calculated by taking the weighted mean, weighted by ratio uncertainty, of the youngest three or more dates that overlap within uncertainty (Coutts et al., 2019). All dates used in maximum depositional age calculations were obtained from $^{206}Pb/^{238}U$ ratios with a probability of concordance >1% and uncertainties were propagated in accordance with the methodology outlined in Horstwood et al. (2016).

[1]GSA Data Repository Item 2020133, File DR1: Raw/full point-counting data, File DR2: All isotopic data from Nanaimo basin, and File DR3: Maximum depositional age plots, is available at http://www.geosociety.org/datarepository/2020, or on request from editing@geosociety.org.

The YGC 2σ method has been demonstrated to produce conservative ages (i.e., rarely younger than the true depositional age of the deposit), especially when derived from large-*n* sample sizes or samples with abundant near-depositional ages (Coutts et al., 2019). Weighted average plots for all samples, including those from Matthews et al. (2017) and Englert et al. (2018), are provided in File DR3 (see footnote 1).

Multi-Dimensional Scaling of U-Pb Detrital Zircon Populations

Multi-dimensional scaling plots are a useful tool for visualizing the statistical differences between large numbers of samples (Vermeesch, 2013; Spencer and Kirkland, 2016). In this study, a single multi-dimensional scaling plot was calculated using detritalPy (Sharman et al., 2018) for all large-*n* detrital zircon samples in the basin, the 22 new samples presented here, and the 27 previously published zircon samples from Matthews et al. (2017) and Englert et al. (2018). Four synthetic age populations (1700, 1380, 150, 90 Ma) were added to the multi-dimensional scaling plot to aid in the visualization of differences between individual samples (Spencer and Kirkland, 2016).

RESULTS

Sandstone Petrology and Point Counting Results

The majority of Nanaimo Group sandstones are arkosic arenites (N = 30) (Table 1) (QFR; Pettijohn et al., 1972). Exceptions include samples DC2, NU3, Or-CO (lithic arenites), Or-HA (sub-litharenite), and Or-EX (subarkose) (Table 1) (QFR; Pettijohn et al., 1972). Samples are largely dominated by feldspathic grains (representing between 7% and 82% of framework grains; mean = 35%), and quartz grains (representing between

TABLE 1. RESULTS OF POINT-COUNTED THIN SECTIONS

Sample name	Sample no.	Quartz	Chert	Feldspar	Micas	Lv	Lm	Ls	Lp	QFR classification	QFL classification
Northern Gulf Islands Transect—Vancouver, Denman, and Hornby islands											
GB4	49	31.4	2.2	30.0	6.0	4.0	7.8	3.8	8.2	Arkosic arenite	Transitional arc
GB3	48	38.7	2.4	28.3	5.8	3.6	8.4	4.2	4.4	Arkosic arenite	Dissected arc
SP2	47	36.8	2.0	30.0	7.1	4.9	6.2	1.1	3.6	Arkosic arenite	Dissected arc
GF3	46	30.4	2.9	32.2	6.2	7.8	8.2	1.3	2.4	Arkosic arenite	Dissected arc
GF1	45	39.1	1.8	32.7	5.3	2.2	6.0	2.9	1.3	Arkosic arenite	Dissected arc
GF2	44	35.8	3.1	29.8	10.0	2.2	4.4	2.0	7.3	Arkosic arenite	Dissected arc
NU3	43	26.2	4.2	24.4	1.6	19.3	10.9	0.2	3.1	Lithic arenite	Transitional arc
DC3	42	30.7	2.0	36.4	0.0	9.8	6.9	0.7	1.3	Arkosic arenite	Dissected arc
DC2	41	22.2	6.7	30.0	2.0	23.6	5.8	1.1	1.8	Lithic arenite	Transitional arc
DC1	40	26.2	3.3	31.1	3.6	14.4	9.3	0.2	2.0	Arkosic arenite	Transitional arc
CD1	38	18.0	4.2	41.3	3.6	8.2	2.4	11.1	2.2	Arkosic arenite	Transitional arc
EX3	36	47.0	13.0	28.3	2.5	4.0	0.0	1.3	4.0	Arkosic arenite	Dissected arc
Central Gulf Islands Transect—Vancouver, Mudge, and Gabriola islands											
GabGBt	33	38.1	2.4	42.0	2.9	8.7	2.9	0.0	2.9	Arkosic arenite	Dissected arc
GabGBm	32	42.3	0.0	42.5	3.5	7.5	0.0	0.0	4.3	Arkosic arenite	Dissected arc
GabSP	29	50.8	1.8	29.5	8.5	1.0	0.0	0.0	8.5	Arkosic arenite	Dissected arc
GabGFt	28	45.3	1.7	40.9	0.6	3.9	0.0	0.3	7.5	Arkosic arenite	Dissected arc
GabDCt	25	19.5	2.3	65.8	10.8	0.5	0.3	0.8	0.3	Arkosic arenite	Basement uplift
GabPRt	23	59.0	6.0	14.6	14.4	2.4	0.0	0.0	0.4	Arkosic arenite	Basement uplift
Southern Gulf Islands Transect—Galiano, Mayne, and Saturna islands											
GalGBt	21	14.9	0.0	50.8	19.3	10.3	0.0	0.5	1.5	Arkosic arenite	Basement uplift
GalGBb2	20	43.7	0.2	42.0	5.7	7.6	0.0	0.2	0.6	Arkosic arenite	Transitional arc
GalGFb	17	41.4	2.5	34.8	9.8	10.0	0.0	0.5	1.1	Arkosic arenite	Transitional arc
MayGBt	16	42.0	1.2	40.0	8.5	4.5	1.0	0.0	1.5	Arkosic arenite	Basement uplift
MayGFb	13	17.4	1.0	64.9	2.3	9.3	2.3	1.0	2.0	Arkosic arenite	Transitional arc
MayDCt	12	27.3	1.3	56.5	6.3	2.5	0.3	0.3	3.5	Arkosic arenite	Basement uplift
MayDCb	11	10.5	0.3	82.3	6.3	0.3	0.0	0.3	0.3	Arkosic arenite	Basement uplift
SatGFt	10	15.3	0.0	69.8	12.1	0.3	0.0	0.0	0.0	Arkosic arenite	Basement uplift
SatGFb	9	28.6	1.0	39.8	6.1	13.0	4.5	0.5	5.5	Arkosic arenite	Transitional arc
SatDCt	8	23.3	0.3	61.6	12.5	1.5	0.0	0.0	1.0	Arkosic arenite	Basement uplift
SatDCb	7	19.6	0.5	69.6	9.8	0.0	0.0	0.0	0.0	Arkosic arenite	Basement uplift
SatDCb2	6	26.6	0.3	55.6	13.1	2.5	1.3	0.0	1.0	Arkosic arenite	Transitional arc
San Juan Islands Transect—Orcas and Sucia islands											
SuCD	5	33.1	17.3	13.9	7.6	1.0	0.0	0.0	0.2	Arkosic arenite	Dissected arc
SuPR	4	45.8	0.5	7.0	18.0	0.5	24.3	0.0	0.0	Arkosic arenite	Transitional arc
OrEX	3	37.5	18.5	20.4	6.0	9.7	7.6	3.2	3.7	Subarkose	Transitional recycled
OrHA	2	48.4	15.3	15.7	2.3	11.5	3.8	0.0	2.9	Sub litharenite	Transitional recycled
OrCO	1	42.3	18.5	12.1	4.4	11.9	7.3	0.2	2.6	Lithic arenite	Transitional recycled

Note: The modal percent of each main framework classification is listed, where some framework classifications are combined (e.g., micas = biotite and muscovite). Full point-counting data is available in Data Repository File DR1 (see text footnote). QFR (quartz, feldspars, rock fragments; Dickinson et al., 1983) and QFL (quartz, feldspar, lithics; Pettijohn et al., 1972) classifications are listed for each sample. Sample number refers to numbers used in Figures 2 and 4. Quartz includes monocrystalline, polycrystalline, and undulatory quartz. Feldspar includes potassium-feldspars and plagioclase. Micas include biotite and muscovite. Lv—volcanic rock fragments; Lm—metamorphic rock fragments; Ls—sedimentary rock fragments; Lp—plutonic rock fragments. Raw point-counting data can be found in File DR1 (see footnote 1).

10% and 50% of counted framework grains; mean = 33%). Chert, micas (biotite and muscovite), and rock fragments (volcanic, plutonic, and metamorphic) are minor components and compose 5% of the framework grains on average (Table 1). Of note, samples of the northern, central, and southern Gulf Islands transects are dominantly composed of feldspathic grains with scarce chert; conversely, samples of the San Juan Islands transect are compositionally distinct and characterized by an increased abundance of chert, and rock fragments, with scarce feldspathic grains (Table 1; Fig. 3).

Nanaimo Group samples populate four fields in the Q_m-F-L_t classification scheme of Dickinson et al. (1983): basement uplift, dissected arc, transitional arc, and transitional recycled (Fig. 3; Table 1). In the northern Gulf islands transect, samples of the DeCourcy Formation plot within the transitional arc field, whereas samples of the Extension, Geoffrey, and Gabriola formations plot within the transitional arc and dissected arc fields (Fig. 3A). In the central and southern Gulf Islands transects, the lower Nanaimo Group and DeCourcy Formation plot within in the basement uplift field (Figs. 3B and 3C). Geoffrey Formation samples plot within dissected and transitional arc fields, except for the Geoffrey Formation exposed on Saturna Island (SatGFt), which plots in the basement uplift field (Fig. 3C; Table 1). Samples of the Geoffrey Formation that plot within the dissected and transitional arc fields have an increased proportion (>5%) of volcanic lithic clasts compared to underlying or overlying basement derived compositions (Table 1). Gabriola Formation samples have compositions that plot within the dissected and transitional arc fields, except for samples of the uppermost Gabriola Formation exposed on Galiano and Mayne Islands (GalGBt, MayGBt), which plot within the basement uplift field (Figs. 3B and 3C; Table 1). In the San Juan Island transect, samples from Orcas Island (Comox, Haslam, and Extension formations) plot within the transitional recycled field, and samples from Sucia Island (Protection and Cedar District formations) plot within the transitional arc and dissected arc fields, respectively (Fig. 3D).

U-Pb Detrital Zircon Geochronology Results

Uranium-lead measurements from 22 samples presented here yielded 4534 dates that passed our filtering criteria. The data presented here combined with the data of Matthews et al. (2017) and Englert et al. (2018) form a basin-wide data set of 49 samples and 10,942 dates. A single PDF is displayed for each of the 49 samples considered (Fig. 4). Proterozoic ages compose 16% of the zircons dated and are dominantly bimodal, ranging from 1900 to 800, with age modes at 1700 and 1380 Ma (Table 2). Paleozoic ages compose 1% of the ages dated and range from 550 to 270 Ma with sample-specific age modes at 260, 350, 400, and 450 Ma. Mesozoic ages compose 82% and have sample-specific age modes at 150, 90, 80, and 75 Ma. Archean ages are rare in the Nanaimo basin, representing 0.2% of dated grains.

Maximum depositional ages for samples presented here range from 144.5 ± 2.0 (SuPr) to 67.7 ± 7 Ma (GabSP) and are listed with the sample

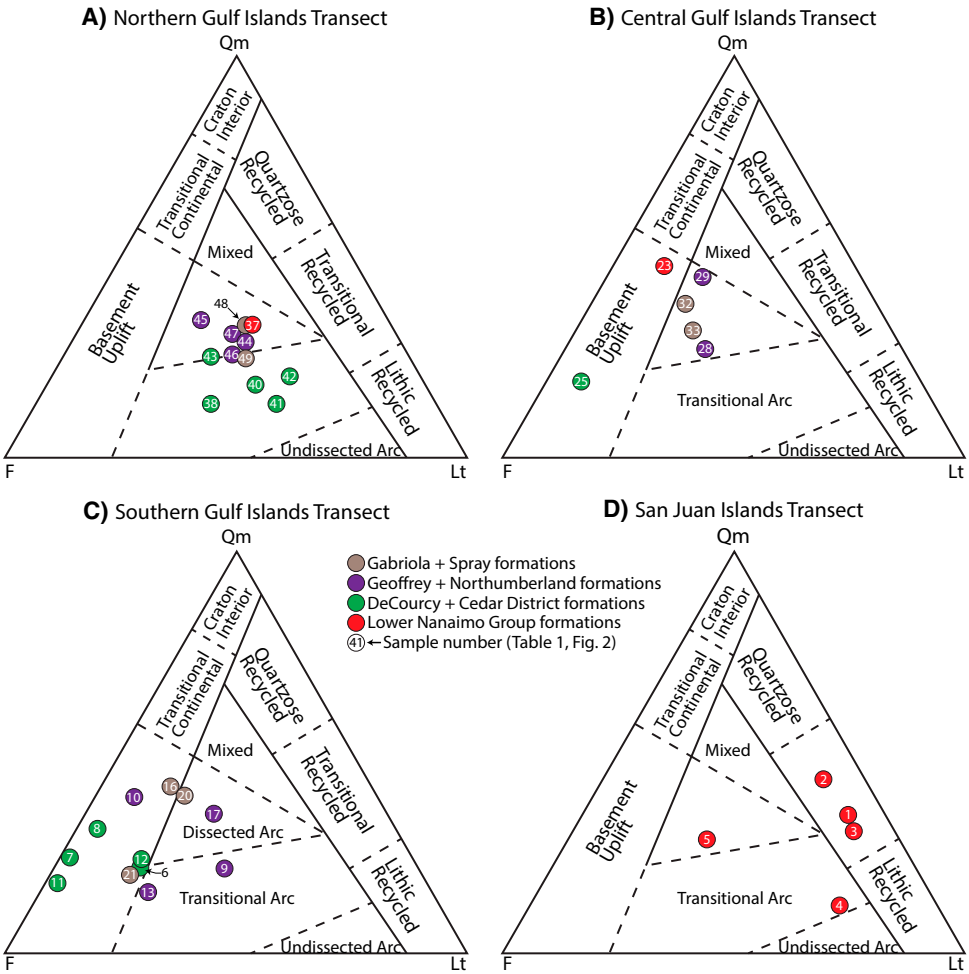

Figure 3. Q_m-F-L_t diagrams for point-counted samples: (A) samples from the northern transect across Vancouver, Denman, and Hornby islands; (B) samples from the central transect across Vancouver, Mudge, and Gabriola islands; (C) samples from the southern transect across Galiano, Mayne, and Saturna islands; and (D) samples of the San Juan islands transect from Sucia and Orcas.

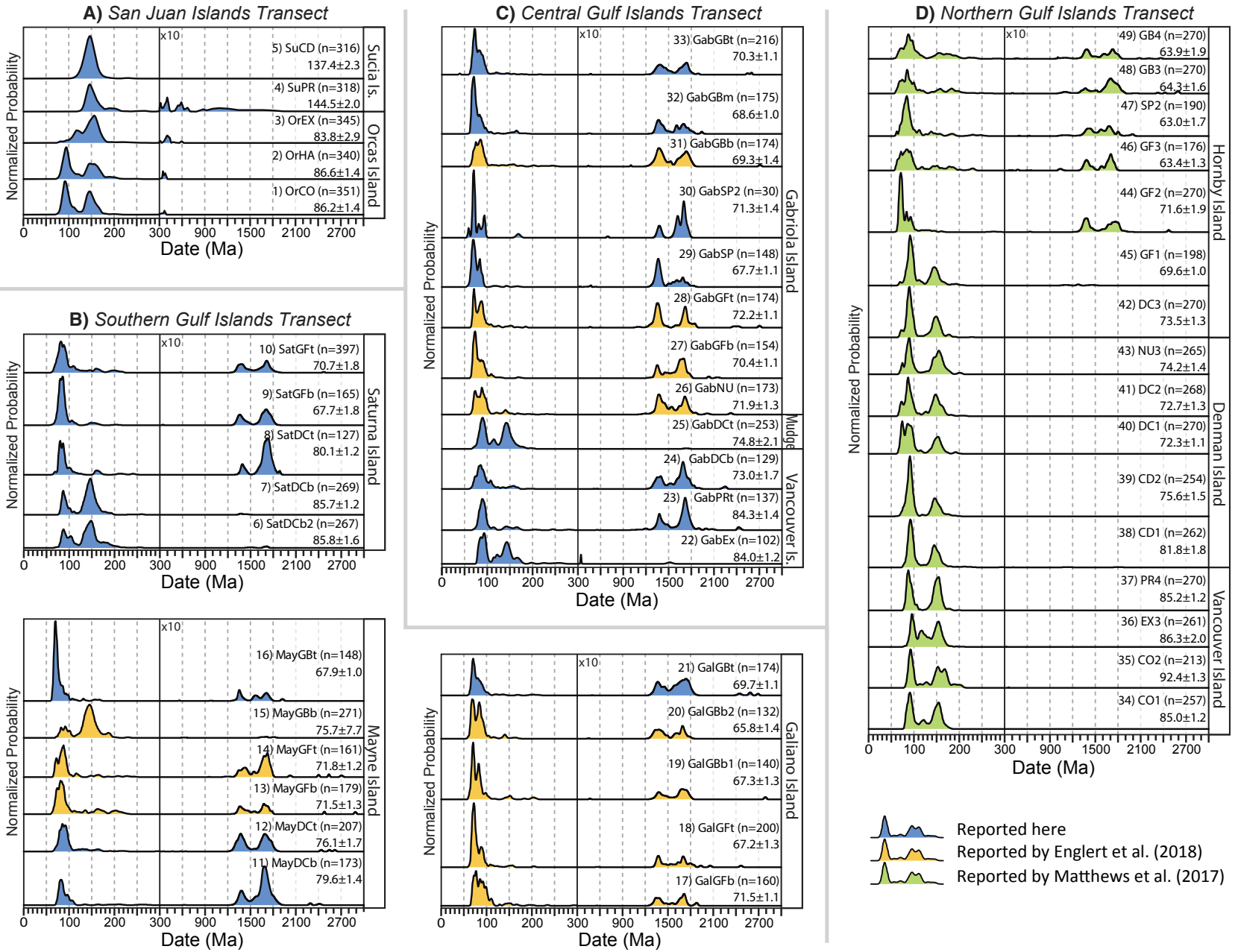

Figure 4. Probability density functions (PDFs) for all samples used to interpret the tectonic and provenance evolution of the Nanaimo Group. (A) San Juan islands transect; (B) southern Gulf Islands transect; (C) central Gulf Islands transect; (D) northern Gulf Islands transect. Samples are organized by stratigraphic position. The maximum depositional age of the sample, calculated by the YGC2σ method of Dickinson and Gehrels (2009), is listed under the sample name and number. Sample numbers correspond to sample locations in Figure 2. Note scale change at 300 Ma. The height of PDFs >300 Ma have been scaled by a factor of 10. Samples reported in Matthews et al. (2017) and Englert et al. (2018) are included with those reported here and color coded respectively.

name in Figure 4. The end of lower Nanaimo Group sedimentation is bracketed by samples PR4 (85.2 ± 1.2 Ma) and GabPRt (84.3 ± 1.2 Ma).

INTERPRETATIONS

Sandstone Petrology and Point Counting Interpretations

We attribute the source and evolution of sediment composition in the Gulf Islands transects (northern, central, and southern) to reflect increased erosion and exhumation of the Coast Mountains Batholith, both through time, and along-strike north-to-south. In the northern Gulf Islands transect, sandstone compositions reflect a shift from transitional arc source regions to dissected arc source regions (Figs. 3A and 5A). We interpret samples from the central and southern Gulf Islands transects to be dominantly derived from uplifted plutonic basement; however, the Geoffrey Formation samples from these transects demonstrate a >5% increase in volcanic lithic fragments and a shift in sandstone composition that reflects erosion of dissected arc source regions. This shift in provenance reflects increased volcanic activity in the Cascade Crystalline core and southern Coastal Mountains Batholith during deposition (e.g., Miller et al., 2009; Cecil et al., 2018) (Table 1; Figs. 3B, 3C, and 5B). Return of sample compositions to basement uplift source terranes by the uppermost Gabriola Formation reflects short-lived hinterland volcanism during the deposition of the Geoffrey Formation (Table 1; Figs. 3B, 3C, and 5B).

We interpret that sandstone compositions of the San Juan Islands transect record the transition from diverse sediment sources in the catchment basin (OrCO, OrHA, OrEX) to more restricted sediment sources (SuPR, SuCD) (Table 1; Fig. 5C). This is documented by a decrease in the variety of framework grains (Table 1; File DR1). The lithic-rich composition, reflected by the transitional- and lithic-recycled sedimentary origin (Fig. 3D), including common chert and exotic framework grains (e.g., amphibole, epidote), suggests derivation from sediment source areas that were not significant for deposits of the Nanaimo Group samples in the Gulf Islands transects yet consistent with sediment sources within the NCTS (e.g., Orcas chert; Pacht, 1984; Brandon et al., 1988) (Table 1; Fig. 5; File DR1).

U-Pb Detrital Zircon Geochronology Interpretations

Detrital Zircon Facies

Five detrital zircon facies are identified based on common age distributions within component zircon spectra, as reflected in a multi-dimensional scaling plot (Fig. 6A), and the presence or absence of key modes in the various samples (Fig. 6B). Zircon facies 1 (F1) is dominated by Mesozoic age grains with modes at 150 and 90 Ma and a minor age mode at 120 Ma. Proterozoic ages are rare (<2%) (Fig. 6; Table 2). Some north-to-south variation is noteworthy in F1 samples, with the northern Gulf Islands transect containing a dominant 90 Ma peak and a subordinate 150 peak, and the southern Gulf Islands transect containing a dominant 150 Ma peak and a subordinate 90 Ma peak (Fig. 4).

Zircon facies 2 (F2) is dominated by Mesozoic age grains that have a primary age mode between 80 and 70 Ma and minor age modes between 250 and 110 Ma. Proterozoic age grains contribute between 15% and 57% of the ages in each sample and have age modes at 1700 and 1380 Ma (Fig. 6; Table 2). This facies varies internally by the prominence of the 90 Ma peak and the age of the youngest grains in each sample (Fig. 4).

Zircon facies 3 (F3) is dominated by Mesozoic age grains that have a bimodal distribution, including age modes at 156 and 115 Ma. Additional minor and discontinuous populations are located between 600 and 300 Ma. Proterozoic age grains constitute ~1% of the facies with ages between 2550 and 1100 Ma. OrEX is the only sample with this signature (Fig. 6; Table 2).

Zircon facies 4 (F4) is dominated by Mesozoic age grains that have a dominant age mode at 146 Ma and a minor age mode at 190 Ma. Paleozoic age grains compose minor modes at 402, 315, and 265 Ma. Proterozoic age grains constitute ~30% of the facies and have broad age distributions that range from 1900 to 800 Ma and 700 to 551 Ma. SuPR is the only sample with this signature (Fig. 6; Table 2).

TABLE 2. PERCENTAGE OF PROTEROZOIC AGES WITHIN EACH SAMPLE, ORGANIZED BY SAMPLE NUMBER AND TRANSECT

Sample name	Sample number	Formation	Detrital zircon facies	% Proterozoic ages
Northern Gulf Islands Transect				
GB4	49	Gabriola	Facies 2	24
GB3	48	Gabriola	Facies 2	40
SP2	47	Spray	Facies 2	25
GF3	46	Geoffrey	Facies 2	25
GF1	45	Geoffrey	Facies 1	1.1
GF2	44	Geoffrey	Facies 2	30
NU3	43	Northumberland	Facies 1	0
DC3	42	DeCourcy	Facies 1	0
DC2	41	DeCourcy	Facies 1	0
DC1	40	DeCourcy	Facies 1	0
CD2	39	Cedar District	Facies 1	0
CD1	38	Cedar District	Facies 1	0.8
PR4	37	Protection	Facies 1	0
EX3	36	Extension	Facies 1	0
CO2	35	Comox	Facies 1	0
CO1	34	Comox	Facies 1	0
Central Gulf Islands Transect				
GabGBt	33	Gabriola	Facies 2	28
GabGBm	32	Gabriola	Facies 2	26
GabGBb	31	Gabriola	Facies 2	37
GabSP2	30	Spray	Facies2	29
GabSP	29	Spray	Facies2	32
GabGFt	28	Geoffrey	Facies 2	22
GabGFb	27	Geoffrey	Facies 2	36
GabNU	26	Northumberland	Facies 2	39
GabDCt	25	DeCourcy	Facies 1	0.4
GabDCb	24	DeCourcy	Facies 2	38
GabPRt	23	Protection	Facies 2	45
GabEX	22	Extension	Facies 1	0.3
Southern Gulf Islands Transect				
GalGBt	21	Gabriola	Facies 2	42
GalGBb2	20	Gabriola	Facies 2	23
GalGBb1	19	Gabriola	Facies 2	22
GalGFt	18	Geoffrey	Facies 2	19
GalGFb	17	Geoffrey	Facies 2	16
MayGBt	16	Gabriola	Facies 2	15
MayGBb	15	Gabriola	Facies 1	1.9
MayGFt	14	Geoffrey	Facies 2	40
MayGFb	13	Geoffrey	Facies 2	20
MayDCt	12	DeCourcy	Facies 2	40
MayDCb	11	DeCourcy	Facies 2	57
SatGFt	10	Geoffrey	Facies 2	21
SatGFb	9	Geoffrey	Facies 2	23
SatDCt	8	DeCourcy	Facies 2	40
SatDCb	7	DeCourcy	Facies 1	0.4
SatDCb2	6	DeCourcy	Facies 1	0.4
San Juan Islands Transect				
SuCD	5	Cedar District	Facies 5	3
SuPR	4	Protection	Facies 4	30
OrEX	3	Extension	Facies 3	0.5
OrHA	2	Haslam	Facies 1	0.9
OrCO	1	Comox	Facies 1	0.9

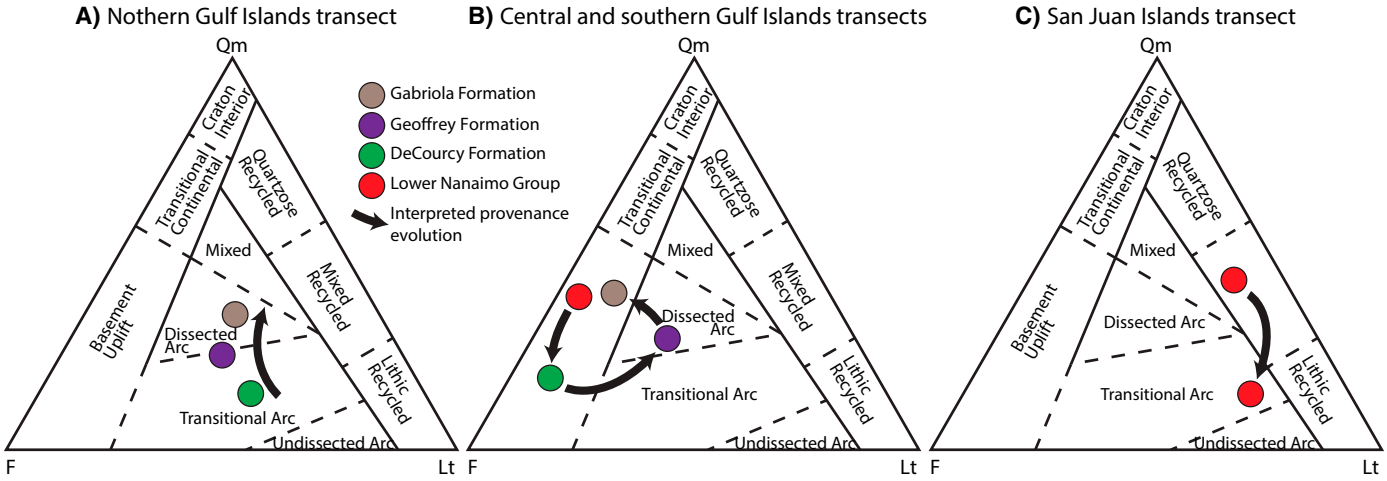

Figure 5. Provenance evolution interpreted for point-counted Nanaimo Group samples plotted on Q_m-F-L_t plots (Dickinson et al., 1983). The composition of individual samples is demarcated by circle color, indicating formation and sample number, relating to Figure 2. (A) Sediment compositions of the northern Gulf Islands transect evolve from compositions associated with transitional arc field to compositions associated with the dissected arc field. (B) Sediment composition of the central and southern Gulf Islands transects are associated with the basement uplift field throughout the lower Nanaimo Group and DeCourcy Formation, with short-lived excursions into compositions that plot within the dissected arc fields in the Geoffrey and lower Gabriola formations. The compositions of uppermost Gabriola Formation samples plot within the basement uplift field. (C) Sediment composition evolution of the San Juan Islands transect evolve from compositions that plot within the transitional recycled field to more lithic-rich compositions in the lithic recycled field.

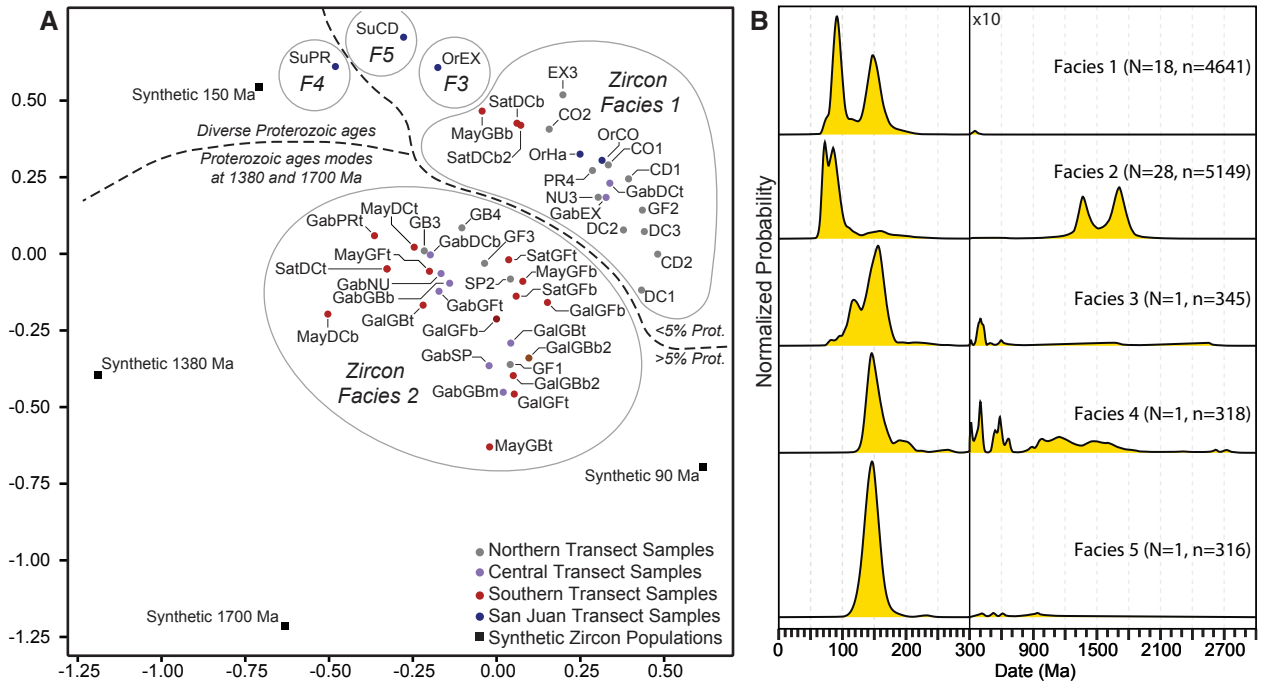

Figure 6. Interpretation of detrital zircon facies within Nanaimo Group samples. (A) Multi-dimensional scaling (MDS) plot of all Nanaimo Group samples from all four transects. Samples are colored by transect. Four synthetic unimodal populations composed of ages common to the Nanaimo Group (i.e., 1700, 1380, 150, 70 Ma) are included. The five interpreted detrital zircon facies are outlined. (B) Probability density functions (PDFs) of the five detrital zircon facies. Note scale break at 300 Ma, as PDFs are scaled by a factor of 10 for ages older than 300 Ma.

Zircon facies 5 (F5) is composed of a single unimodal zircon population centered at 150 Ma, ranging from 229 to 111 Ma. Remaining Phanerozoic age grains range from 522 to 415 Ma. Proterozoic and older grains range from 2000 to 1700 Ma and 1200 to 900 Ma. Non-Mesozoic ages constitute ~3% of the facies. SuCD is the only sample with this signature (Fig. 6; Table 2).

Provenance of Crystalline Zircon Ages

Detrital zircon ages of the Nanaimo basin range from 58.7 to 2888.5 Ma and are plausibly derived from crystalline sources that reflect much of the geologic record of North America. However, as zircon is highly resistant to chemical and physical abrasion, it may be recycled multiple times through various geologic processes (e.g., Fedo et al., 2003; Hadlari et al., 2015). Therefore, zircon grains in the Nanaimo basin may have ultimately derived from the crystalline sources discussed below but were subsequently recycled from other sedimentary units prior to being deposited in the basin.

Proterozoic zircon populations in F2 (e.g., 1850–1560 and 1450–1300 Ma) may derive from rocks that make up much of the basement of Laurentia. Zircon with these ages are common in the Yavapai and Mazatzal terranes (1790 and 1610 Ma) (Whitmeyer and Karlstrom, 2007), Granite Rhyolite Province, additional A-type granites (1490 and 1310 Ma) (Goodge and Vervoot, 2006), and the Grenville orogen (1370 and 1000 Ma) (Whitmeyer and Karlstrom, 2007). Proterozoic ages of F4 (e.g., 1700–541 Ma) may derive from similar sources as F2 with the addition of Appalachian and Caledonides orogens (850–541 Ma) (Anfinson et al., 2012).

The Paleozoic zircon populations found in Nanaimo Group samples (i.e., modes at 450, 400, and 350 Ma) are rare in crystalline rocks of North America. Zircons of this age (i.e., 450–350 Ma) are found in oceanic and continental volcanic arcs within the Caledonian and Ellesmerian orogens (Anfinson et al., 2012). Rocks of the Alexander Terrane have age modes that range from 460 to 415 Ma (White et al., 2016). Orthogneiss within the Yellow Aster Complex range in age from 406 to 410 Ma (Schermer et al., 2018). Intrusive dykes within the Yellow Aster Complex and Turtleback terrane range in age from 418 to 375 Ma. (Brown et al., 2010; Schermer et al., 2018). Volcanic strata of the Sicker Group, a dominant portion of the Wrangellia terrane, range in age from 370 to 340 Ma (Sluggett, 2003).

Mesozoic to early Paleogene age zircon found in all Nanaimo Group detrital zircon facies are common to volcanic and plutonic rocks of western North America. The Wrangellia terrane is composed of multiple Late Triassic to Late Jurassic units, including the Karmutsen Formation (ca. 220 Ma), Bonanza Formation (ca. 202–165 Ma), and the Island Intrusions–West Coast Crystalline Complex (ca. 190 and 167 Ma) (DeBari et al., 1999; Greene et al., 2010; Canil et al., 2013). The magmatic history of the Coast Mountains Batholith spans much of the Mesozoic (Cecil et al., 2018). Plutonism in the Coast Mountains Batholith spans 200–60 Ma (Cecil et al., 2018), with previously discussed age modes representative of regional high-flux magmatic events (e.g., Friedman and Armstrong, 1995; Miller et al., 2009; Cecil et al., 2018).

Sediment Source Areas for Nanaimo Group Detrital Zircon Facies

Detrital zircon facies 1 (F1) is composed of Mesozoic zircon grains that we interpret to derive from the Coast Mountains Batholith, as the range of ages and modes coincides with high-flux events within the southern and Vancouver Coast Mountains Batholith, as well as the Cascade Crystalline Core (CCC) (90 and 150 Ma age modes) (Fig. 6) (Friedman and Armstrong, 1995; Miller et al., 2009; Cecil et al., 2018). Zircon age populations that compose the Paleozoic mode in samples OrCO, OrHA, and GabEX (ca. 350 Ma) are interpreted herein to derive from the underlying Sicker Group of the Wrangellia Terrane (Figs. 4A and 4C).

Detrital zircon facies 2 (F2) is composed of Mesozoic grains that we interpret to derive from the Coast Mountains Batholith and Proterozoic ages that derive from sediment sources east of the arc (Figs. 6 and 7A) (Matthews et al., 2017; Englert et al., 2018). We interpret grains yielding latest Cretaceous ages to derive from the CCC and southern Coast Mountains Batholith, where plutonism continued until 71 Ma (Miller et al., 2009) and post–60 Ma (Cecil et al., 2018), respectively. Previously interpreted sources of Proterozoic detrital zircon characteristic of F2 samples (1700 and 1380 Ma age modes) (e.g., Belt-Purcell basin, Lemhi sub-basin, of Idaho and Mojave-Sonoran region of SW North America) are still applicable, and the data presented here do not refine the sediment source interpretation.

Detrital zircon facies 3 (F3) is composed of grains that we interpret to derive from the NCTS with minor contribution from the Coast Mountains Batholith. We interpret zircon grains yielding ages that fall within the 120 Ma and 150 Ma age modes to derive from the Bell Pass mélange and rocks of the Shuskan/Haystack nappes, respectively (Fig. 7). Zircon grains yielding ages ca. 85 Ma are interpreted here to derive from the Coast Mountains Batholith, as Late Cretaceous ages are rare in the NCTS. We interpret Paleozoic age grains to be sourced from the Chilliwack Terrane, Turtleback Complex, or Yellow Aster Complex of the Chilliwack nappe, which all contain prominent ca. 400 Ma age modes (Fig. 7). Proterozoic age zircon grains in F3 are rare (1%); however, we interpret them to derive from the NCTS as they have a large range of ages similar to that of Yellow Aster Complex (2000–900 Ma), and dissimilar age range and age modes to the Proterozoic ages of F2 (Fig. 6). The age modes present in F3 are similar to the age distribution of detrital zircons found in Nanaimo basin strata on Barnes Island reported by Brown (2012) (Fig. 7). Brown (2012) interpreted source areas within the NCTS (i.e., Yellow Aster and Turtleback complexes) for the Barnes Island samples, based on zircon age modes and petrologic analysis of clasts.

We interpret detrital zircon facies 4 (F4) to derive from rocks of the NCTS. A preponderance of grains yielding latest Jurassic to Early Cretaceous ages (150 Ma age mode) and an absence of grains younger than 100 Ma (Figs. 5B and 5C) are attributed to sediment recycling from the Shuskan and Haystack nappes (Fig. 7). Sedimentary rocks with nearly unimodal zircon age modes at ca. 150 Ma (Figs. 5B and 5C) is consistent with this interpretation, rather than derivation from the Coast Mountains Batholith. Paleozoic ages in F4 (400 Ma age mode) may derive from a variety of strata within the Chilliwack nappe (i.e., the Yellow Aster complex, Turtleback complex, and Chilliwack terrane) and Orcas nappe (i.e., Bell Pass mélange) where these ages are common (Fig. 7). Lastly, detrital zircon facies 4 samples contain a small number of Proterozoic ages that are interpreted herein to derive from the Yellow Aster Complex as they are dissimilar to those found in Facies 2 (i.e., larger range of ages, and lack of bimodal distribution) (Figs. 6 and 7).

We interpret detrital zircon facies 5 (F5) to derive from rocks of the NCTS. The facies is composed of a single age mode at ca. 150 Ma and component grains that we interpret to derive entirely from strata of the Shuskan and/or Haystack nappes (Fig. 7). Absence of younger, mid-to-Late Cretaceous ages suggests that derivation from the Coast Mountains Batholith is unlikely.

The Nanaimo Group deposits exposed along the northern transect are characterized by F1 and F2 detrital zircon populations, and the transition between F1 and F2 occurs ca. 71 Ma. The Nanaimo Group deposits exposed in the central and southern transects are characterized by F1 and F2 detrital zircon populations; however, the transition between F1 and

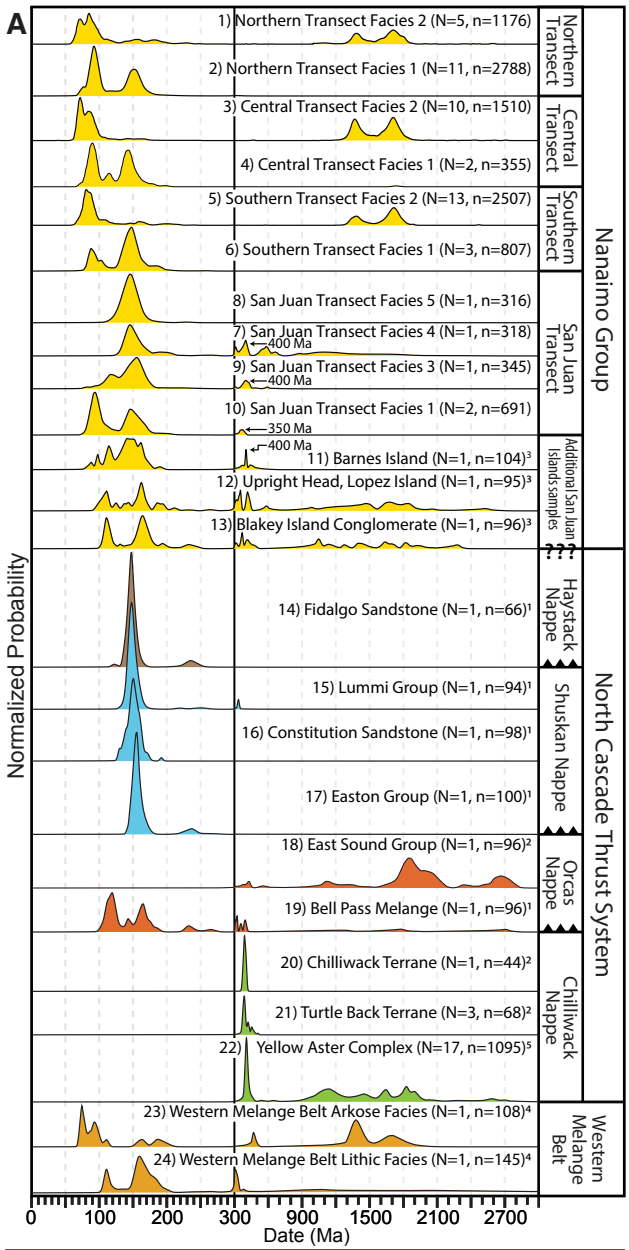

Figure 7. Comparison of detrital zircon age distributions to potential source areas in the North Cascade thrust system (NCTS). (A) Probability density functions (PDFs) of Nanaimo Group samples grouped by facies (PDFs 1–13) and potential source terranes in the NCTS (i.e., PDFs 14–24). Note scale break at 300 Ma. PDFs are scaled by a factor of 10 for ages older than 300 Ma, except for the Turtleback and Yellow Aster Complex PDFs, which are not scaled. Superscript labels denote data source: [1]Brown and Gehrels (2007); [2]Brown et al. (2010); [3]Brown (2012); [4]Sauer et al. (2017); [5]Schermer et al. (2018). (B) A simplified geologic map of potential sediment source areas within the NCTS. Map modified from Brown and Gehrels (2007).

F2 occurs ca. 84 Ma. Lastly, the Nanaimo Group deposits exposed in the San Juan Island transect are characterized by F1, F3, F4, and F5 detrital zircon populations. The transition from F1 to F3 occurs ca. 84 Ma, while the transition from F3 to F4 and later F5 occurs post–84 Ma (Fig. 4).

DISCUSSION

Influence of the North Cascade Thrust System on the Nanaimo Basin

Previous models for provenance evolution of the Nanaimo Group have interpreted the NCTS as a major sediment source and driver of sediment transfer to the southern Nanaimo basin (e.g., Pacht, 1984; Mustard, 1994). These interpretations are largely based on the identification of distinct clasts in the Nanaimo Group that are interpreted to derive from units within the NCTS (e.g., Vance, 1975; Pacht, 1984; Brown, 2012). The most widespread of these are radiolarian chert clasts interpreted to derive from the Triassic to Lower Jurassic Orcas Chert of the Orcas nappe (Fig. 7), which have been identified in the lower Nanaimo Group as far north as the Cowichan River area (Fig. 1) (Pacht, 1984). Other exotic clasts that are interpreted to be sourced from the NCTS (e.g., clasts of metamorphic rock in Nanaimo Group equivalents exposed on Sucia, Saturna, and Waldron islands) are much more localized to the southernmost portions of the Nanaimo basin (Pacht, 1984; Brown, 2012).

Our petrographic and detrital zircon data refines these interpretations and suggest that sediment shed from the NCTS (i.e., F3, F4, and F5) was deposited in a spatially restricted part of the Nanaimo basin, immediately adjacent to the NCTS. These data demonstrate that while chert clasts are common within the Comox, Haslam, and Extension formations in the San Juan Island transect, the remainder of the Nanaimo Group is largely devoid of chert (Table 1). Furthermore, detrital zircon facies that we interpret to derive from the NCTS (F3, F4, F5) are limited to the San Juan Island transect (Figs. 6 and 7). Interestingly, samples from the San Juan Islands transect that are most chert-rich (e.g., OrCO, OrHA) exhibit the same F1 detrital zircon signatures as chert-poor samples of the Nanaimo Group from elsewhere in the basin (e.g., CO1) (Figs. 4 and 6).

If the NCTS only contributed sediment to the southernmost part of the Nanaimo basin, an alternative source is needed for the small quantities of chert found within the lower Nanaimo Group exposed far from the NCTS (e.g., GabPRt, EX). It is possible that chert in the lower Nanaimo Group derived from minor chert units within strata of Wrangellia (Pacht, 1984; Brandon et al., 1986), which is thought to have formed basement highs that controlled sedimentation of the lower Nanaimo Group (Pacht, 1984; Mustard, 1994; Kent et al., 2019), as well as acted as a sediment source (Huang et al., 2019). The lack of chert in the upper Nanaimo Group in these regions could signal burial of Wrangellian basement during progressive onlap of the basal unconformity during deposition of lower Nanaimo Group (Johnstone et al., 2006; Kent et al., 2019). Taken

together, our data suggest a relatively minor influence of the NCTS as a sediment source and driver of the Nanaimo basin evolution. Although the NCTS was emplaced prior to or during Nanaimo Group deposition, it only supplied sediment to the southernmost portion of the basin with little impact on the basin as a whole. Contraction within the NCTS may have caused enhanced subsidence locally within the southern portion of the basin; however, contraction in the Coast Mountains Batholith ended prior to the deepening of the Nanaimo basin (e.g., Journeay and Friedman, 1993; Rusmore and Woodsworth, 1994). As such, an additional driver for basin-wide subsidence ca. 84 Ma must have been important.

Implications for North Cascade Thrust System Emplacement Timing

There is disagreement regarding the timing and mode of tectonic emplacement of the NCTS, and its role in basin geodynamics. Brandon et al. (1988) suggested that the NCTS were assembled during a single event synchronous with the collision of the Insular Superterrane during the latest Jurassic and Early Cretaceous, then uplifted during the Late Cretaceous ca. 84 Ma. In contrast, Brown (2012) used maximum depositional ages and detrital zircon age distributions of sedimentary bodies within the NCTS (e.g., Barnes Island, Upright Head) to suggest the NCTS was assembled via sequential emplacement of structurally higher nappes onto the southern margin of the basin.

Our detrital zircon and petrographic data provide new constraints on the timing and sequence of nappe emplacement. The lowermost Nanaimo Group deposits of the San Juan Island transect (OrCO and OrHA; 87–86 Ma) contain detrital zircons interpreted to derive from the Coast Mountains Batholith (F1); however, they contain abundant chert that has previously been interpreted to derive from the Orcas nappe, suggesting the Orcas and Chilliwack nappes may have been emplaced by that time (cf. Brown, 2012). If the chert found in these lowermost samples derives from the Orcas nappe, then the underlying Chilliwack nappe was not a significant sediment source at this time as few ca. 400 Ma grains and no Proterozoic grains are present in these samples. The earliest detrital zircon evidence of NCTS uplift is found in the Extension Formation on Orcas Island (F3) ca. 84 Ma, where sediment is dominantly derived from the lower nappes (i.e., Chilliwack and Orcas). During deposition of the Protection and Cedar District Formations on Sucia Island (ca. 83 Ma; Ward et al., 2012) sediment was derived from upper nappes (i.e., Haystack nappes).

The data provided here demonstrates sequential thrusting of NCTS terranes onto the southern margin of the basin, consistent with the model of Brown (2012). The lowermost nappes (Chilliwack and Orcas) were emplaced by 84 Ma, but it is plausible they were emplaced earlier but only the Orcas chert was eroded into the basin. From ca. 84 to ca. 83 Ma the remaining nappes were emplaced (i.e., Shuskan and Haystack nappes), covering the lower nappe, with subsequent sediment derived only from the structurally highest units. In the model of Brandon et al. (1988), where construction of the nappe pile occurred elsewhere along the margin and was thrust into contact with the Nanaimo basin, detrital zircon age populations would either be sourced from the highest structural levels first, or simultaneously from all structural levels, depending on the geometry of the nappe pile.

Stratigraphic Record of Sediment Underplating

The transition from detrital zircon F1 to F2 (i.e., shift to inclusions of significant Proterozoic dates) in the Nanaimo basin occurs diachronously throughout the basin. Previously, Matthews et al. (2017) observed that F2 detrital zircon populations were introduced to the northern Gulf Island transect at the onset of Geoffrey Formation deposition, 71.6 ± 1.9 Ma (Fig. 4C). Englert et al. (2018) demonstrated that F2 detrital zircon populations sourced from east of the Coast Mountains Batholith occurred synchronously with deposition of the Geoffrey Formation (ca. 71 Ma), which is characterized by the basin-wide deposition of large gravel-filled submarine channel-system deposits. The data presented here demonstrates that the introduction of F2 detrital zircon populations occurs 10–15 m.y. earlier in the central and southern Gulf Islands transects (ca. 84 Ma). This observation requires that the mechanism(s) responsible for the transition from F1 to F2 detrital zircon populations in the central and southern portions of the basin (e.g., fluvial drainage expansion) are different from the mechanism that controlled basin-wide gravel dispersal during deposition of the Geoffrey Formation.

Previous authors have discussed the similarity between the detrital zircon age distributions of the Swakane Gneiss and Nanaimo Group, but no definitive correlation between them has been made (e.g., Matzel et al., 2004; Sauer et al., 2018). Correlation is difficult as the Swakane Gneiss is composed of forearc/trench sediments that were incorporated into the Coast Mountains Batholith at depths of ~40 km, and subsequently metamorphosed (Matzel et al., 2004, Sauer et al., 2018). Sauer et al. (2018) demonstrated that the Swakane Gneiss contains two dominant detrital zircon populations, which are very similar to F1 and F2 described here: (1) rocks yielding maximum depositional ages >84 Ma are characterized by populations with Mesozoic age modes at 90, 110, and 150 Ma (Fig. 8A); and (2) rocks yielding maximum depositional ages <84 Ma are characterized by populations with major age modes at 70 and 80 Ma, minor modes at 90 and 110 Ma, sparse ages between 110–300 Ma, and Proterozoic age populations between 1800 and 1600 and 1440–1360 Ma (Sauer et al., 2018) (Fig. 8A). The similarity between detrital zircon populations in the Swakane Gneiss and those of the Nanaimo Group, as well as the similarity in the timing of the transition from F1 to F2 age distributions within the Swakane Gneiss (ca. 86 and 84 Ma) and the Southern Nanaimo basin (ca. 84 Ma) suggest they share a similar provenance (Fig. 8A). We propose that the protolith of the Swakane Gneiss was either derived from the same sediment sources as the Nanaimo Group and deposited elsewhere along the Pacific margin, or was composed of Nanaimo Group sediments.

The mechanism for burial of the Swakane Gneiss to lower-crustal depths (~40 km) (Valley et al., 2003; Matzel et al., 2004) is uncertain, and both underplating of trench sediments to the base of the CCC and underthrusting of a forearc region under or into the CCC have been proposed (Matzel et al., 2004; Sauer et al., 2018). Sauer et al. (2019) demonstrated that the Swakane Gneiss had very similar isotopic properties (e.g., U-Pb and Lu-Hf) to well-studied underplated schists exposed in California, suggesting that underplating may have occurred. However, clockwise *P-T* pathways (Valley et al., 2003; Matzel et al., 2004), and ongoing local magmatism (Miller et al., 2009), neither of which are found in the Californian schists, support an underthrusting mechanism.

We propose a model that details the interaction between CCC deformation and Nanaimo basin sedimentation. The Swakane Gneiss protolith was deposited between 91 and 81 Ma, was sourced from similar sediment source terranes as the Nanaimo basin, and was later incorporated into the arc, reaching maximum metamorphic conditions between 72 and 66 Ma (Sauer et al., 2018). Regardless of the mechanism interpreted to incorporate the Swakane protolith into the CCC, uplift associated with either underthrusting or underplating drove basin sedimentation and culminated in gravel deposition characteristic of Geoffrey Formation, ca. 72 Ma (Fig. 8B). Additionally, the onset of gravel deposition in the Nanaimo basin and peak metamorphic conditions of the Swakane (ca. 72 Ma) are coincident with an increase in exhumation rate in the CCC from 0.6 to 3 mm/yr (Paterson et al., 2004) (Fig. 8B). Identifying the response of sedimentation (see Englert et al., 2018) to changes in lower

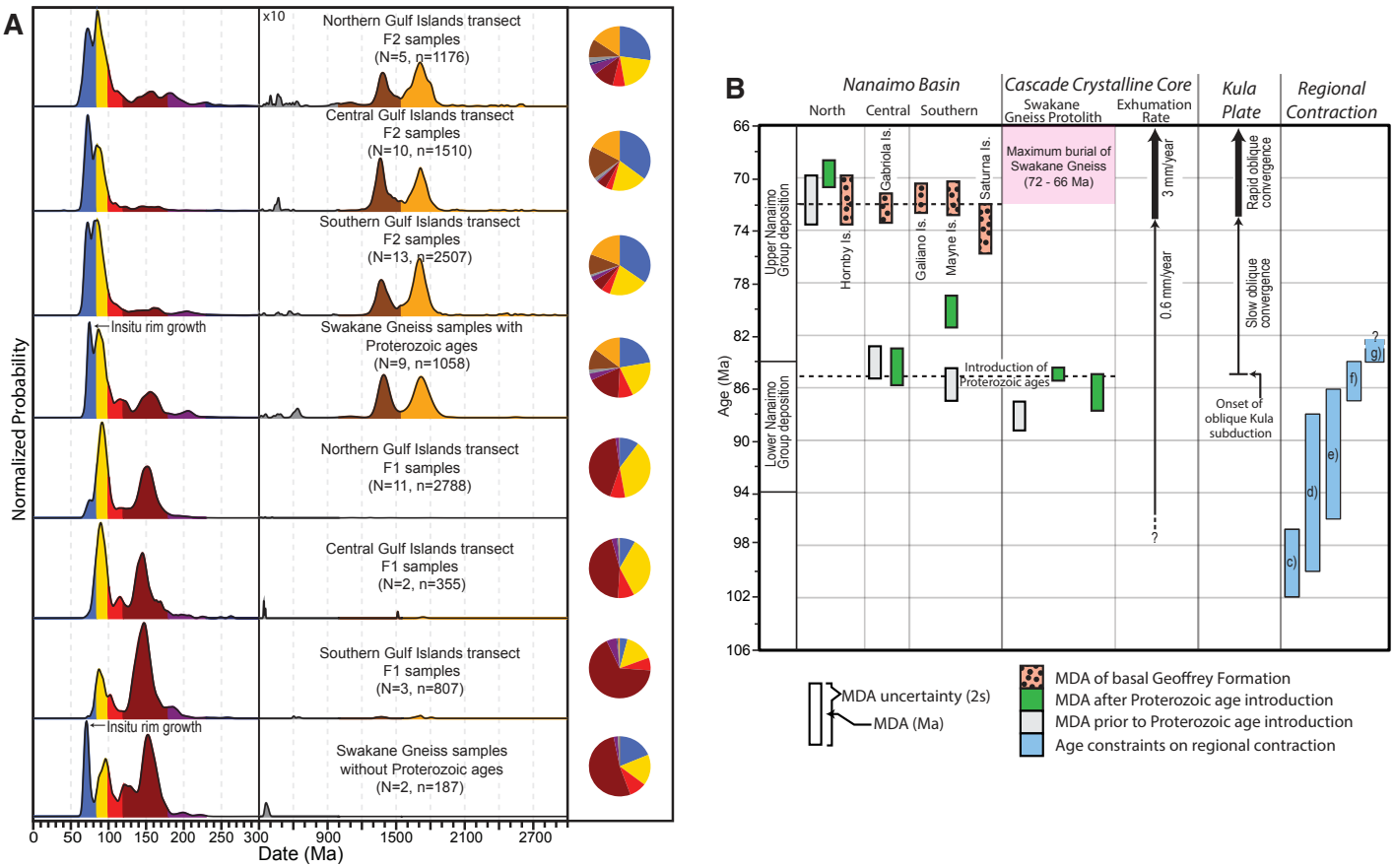

Figure 8. Comparison of Nanaimo basin with Swakane Gneiss detrital zircon data. (A) Comparison of detrital zircon age distributions for the Nanaimo basin transects and the Swakane Gneiss. Samples are grouped by the presence or absence of Proterozoic ages within the sample population. 0 < blue ≤ 85, 85 < yellow ≤ 100, 100 < red ≤ 120, 120 < burgundy ≤ 180, 180 < purple ≤ 230, 230 < navy ≤ 300, 300 < grey ≤ 1000, 1000 < brown ≤ 1600, 1600 < gold ≤ 2500. Note scale break at 300 Ma. Probability density functions are scaled by a factor of 10 for ages older than 300 Ma. (B) Timing of the introduction of Proterozoic ages into the Nanaimo basin and protolith of the Swakane Gneiss. Maximum burial of the Swakane Gneiss and exhumation rates of the Cascade Crystalline Core are included from Matzel et al. (2004) and Paterson et al. (2004), respectively. Swakane Gneiss detrital zircon data from Sauer et al. (2018). Kula convergence is retrieved from Woods and Davies (1982) and Doubrovine and Tarduno (2008). Constraints on regional contraction are from (c) Harrison Lake thrust belt (Journeay and Friedman, 1993), (d) East Cascade Fold belt (McGroder, 1989), (e) Taseko Lake-Bridge River Thrust Belt (Schiarizza et al., 1990), (f) East Waddington thrust belt (Rusmore and Woodsworth, 1994), (g) North Cascade Thrust Belt (Brandon et al., 1988; data presented here). MDA—maximum depositional age.

plate dynamics, identified here, is important, as the response of sediment routing systems to underplating or under thrusting is difficult to quantify in both ancient (Sierra Nevada, California; Ducea and Chapman, 2018) or modern (Raukumara Range, New Zealand; Bassett et al., 2010; Coast Cordillera, Chile; Encinas et al., 2012) settings.

Paleogeography of the Southern Insular Superterrane during the Late Cretaceous

The basin-wide data set presented here demonstrates two basin-scale events recorded in the strata of the Nanaimo Group; the first event occurred ca. 84 Ma and the second ca. 72 Ma (Fig. 9). The first basin-scale event included: (1) the onset of basin-wide deep-water sedimentation (i.e., transition between lower and upper Nanaimo Group), (2) a transition in detrital zircon facies from F1 to F2 across the central and southern Nanaimo basin as well as the protolith of the Swakane Gneiss, and (3) uplift of the NCTS with sediment shed into a restricted portion of the basin (Figs. 9A, 9B, and 9E). We hypothesize that the tectonic driver for this event is the onset of oblique subduction of the Kula plate, which rifted from the Farallon plate and began subducting obliquely beneath the Nanaimo basin as early as 85 Ma (Woods and Davies, 1982; Engebretson et al., 1984). Oblique subduction can increase the rate of subduction erosion causing forearc subsidence (von Huene and Scholl, 1991; Fildani et al., 2008), along with driving forearc deformation and uplift opposite to the direction of subduction (i.e., uplift at the southern end of the Nanaimo basin) (Malatesta et al., 2013, 2016). This process may have driven the transition between F1 to F2 detrital zircon populations in the central and southern Nanaimo basin transects.

The second distinct event occurred at 72 Ma and included: (1) basin-wide introduction of gravel to the basin, as recorded by the Geoffrey Formation (Englert et al., 2018), (2) the change from F1 to F2 detrital zircons facies in the northern Gulf Islands transects, (3) emplacement and metamorphism of the Swakane Gneiss (Sauer et al., 2018), and (4) increased exhumation rate of the CCC (Paterson et al., 2004; Figs. 9C–9E). Detrital zircon samples from this event record a high abundance of near-depositional ages, and sandstone compositions from the

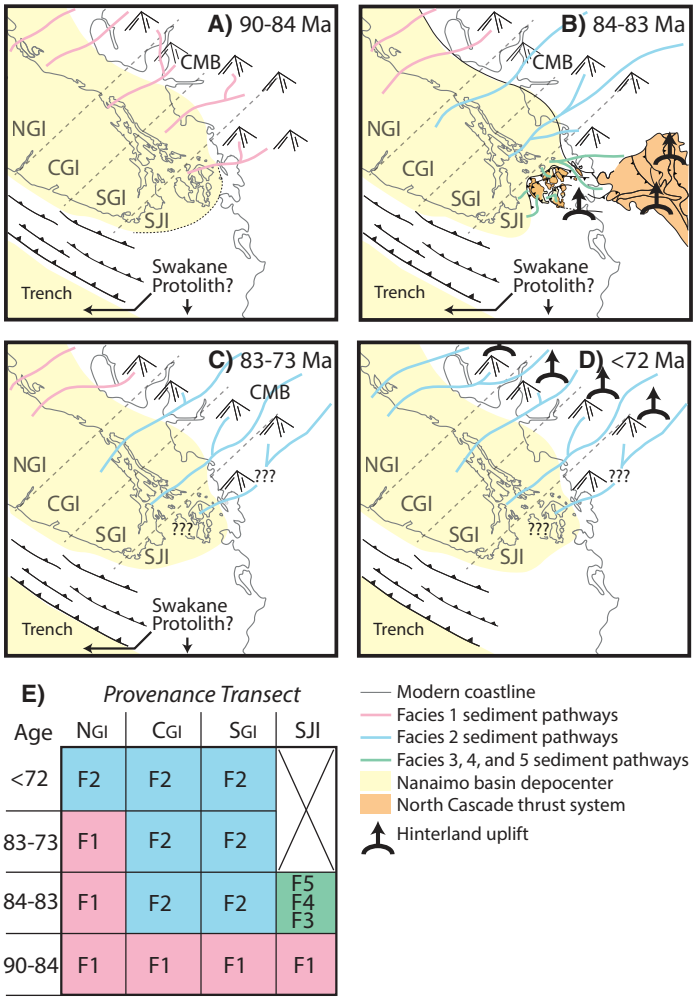

Figure 9. Paleogeographic maps of the Nanaimo basin demonstrating along-strike variability of sediment provenance and the timing of the two basin-wide events identified in this study, ca. 84 and 72 Ma. CMB—Coast Mountains Batholith; CGI—central Gulf islands; NGI—northern Gulf islands; SGI—southern Gulf islands; SJI—San Juan islands.

central and southern Gulf Islands transects record an increase in volcanic rock fragments. We speculate that these processes may have been caused by an increase in the rate of Kula plate subduction and obliquity starting at 73 Ma, as documented by Doubrovine and Tarduno (2008).

Events in the Nanaimo basin reflect the timing of Kula plate formation, along with changes in convergence and obliquity of subduction. Our results indicate that changes in subduction have a regional impact and are a dominant control on forearc basin evolution; however, they may manifest differently across the basin due to along-strike variability of these processes. Our data suggest that the lower plate had a dominant influence on the evolution of the basin, which is inconsistent with the foreland model of the basin (cf. Mustard, 1994). Due to this interaction and the correlation between changes in Kula Plate spreading with basin and hinterland events, we conclude that the Nanaimo basin should be considered a forearc basin.

The identification of the events at ca. 84 Ma and ca. 72 Ma, as well as their relationships to the history of the Kula Plate is important for understanding the Late Cretaceous paleogeography of the Pacific margin of North America. The formation of the Kula plate has been invoked for the northward translation of the Baja-BC block (e.g., Umhoefer, 1987; Beck, 1991) and the events documented here may record initial excision and or docking of the block. The Kula-Farallon ridge is interpreted to have formed south of the Nanaimo basin (Woods and Davies, 1982; Engebretson et al., 1985; Doubrovine and Tarduno, 2008; Seton et al., 2012). However, if the Nanaimo basin, as a part of the Baja-BC Block, was located at the latitude California during the Late Cretaceous (e.g., Housen and Beck, 1999; Matthews et al., 2017; Sauer et al., 2019), then the Kula-Farallon ridge was located in southern California or northern Mexico at 85 Ma. This position of the ridge is consistent with oceanic plate reconstructions proposed by Engebretson et al. (1985); however, this is inconsistent with paleogeographic models for the southwestern North America during the Late Cretaceous (Jacobson et al., 2011; Sharman et al., 2015; Yonkee and Weil, 2015), which generally favors a higher latitude for both the Baja-BC block and the Kula-Farallon ridge north of California in the latest Cretaceous. A northerly position for the Baja-BC block would allow for the Kula-Farallon ridge to form north of California (e.g., at the latitude of northern Oregon or Washington; Doubrovine and Tarduno, 2008; Seton et al., 2012). Regardless of proposed paleolatitude, the Baja-BC block was located south of its current position in the Late Cretaceous (e.g., Wyld et al., 2006). The events identified here at 84 Ma and 72 Ma, as well as other events (e.g., subduction of the Kula-Farallon Ridge), should be recorded in units outside the Baja-BC block, providing evidence for its paleolatitude.

CONCLUSIONS

Thirty-five point-counted sandstone thin sections and 22 new U-Pb detrital zircon samples complete a basin-wide north-to-south perspective of provenance evolution in the Nanaimo basin of western British Columbia, Canada, and northern Washington, USA. Samples are divided into Gulf Islands transects (northern, central, and southern) and a transect through the San Juan Islands. Petrologic trends in the Gulf Islands transects demonstrate increased exhumation of the Coast Mountains Batholith both through time and from north to south along the margin of the basin. Evolution of sediment composition in the San Juan Islands transects reflects derivation from various thrust nappes of the North Cascade thrust system (NCTS) during their construction early in the basin's history.

The basin-wide detrital zircon data set incorporates data from previous studies (N = 49, n = 10,942), and is characterized by five detrital zircon facies (F1–F5). These facies are interpreted to represent sediment derivation from the Coast Mountains Batholith, hypothesized sediment sources east of the Coast Mountains Batholith, NCTS, and Wrangellia basement. The Nanaimo basin is largely dominated by sediment derived from the Coast Mountains Batholith (F1) and sources east of the Coast Mountains Batholith (F2). Because the detrital zircon age distributions, as well as the change between F1 and F2 zircon populations observed in the majority of the Nanaimo basin (ca. 84 Ma) occurs synchronously in the protolith of the Swakane Gneiss, we suggest that the protolith of the Swakane Gneiss was derived from similar sources or was composed of Nanaimo Group sediments. Sediment derived from the NCTS (F3, F4, and F5) was deposited in a spatially restricted zone, directly adjacent to the NCTS, rather than distributed across the Nanaimo basin, as suggested by previous models.

Two large, basin-scale tectonic events are resolved in this data set. The first event ca. 84 Ma included deepening of the basin, a change in detrital zircon age distributions, and uplift of the NCTS. This event is hypothesized to be driven by onset of oblique Kula Plate subduction. The second event included basin-wide coarse-grained sedimentation, localized high-flux events, increased exhumation of the CCC, and the underplating

and metamorphism of the Swakane Gneiss at ca. 72 Ma. These events are important for future paleographic reconstructions of the Pacific margin, as they may represent key processes involved in northward translation of the Baja-BC block. Additionally, they highlight the interplay between oblique subduction, underplating or underthrusting, and basin sedimentation, which is applicable to other modern and ancient forearc settings.

ACKNOWLEDGMENTS

Funding for this research was provided by a Natural Sciences and Engineering Research Council (NSERC) Discovery Grant (No. RGPIN/341715-2013) to S. Hubbard and a Queen Elizabeth II scholarship from the University of Calgary to D. Coutts. We would like to thank residents of the Gulf Islands and San Juan Islands for access to private property, Washington State Parks for permission to conduct field work in Sucia Island State Marine Park, and Nate Averna for help with transport to Sucia Island. The manuscript evolved thanks to insightful discussions with John Garver and Mark Brandon, as well as constructive reviews from Sarah Roeske, Kathleen Surpless, and Andrew Leier.

REFERENCES CITED

Anfinson, O.A., Leier, A.L., Gaschnig, R., Embry, A.F., and Dewing, K., 2012, U-Pb and Hf isotopic data from Franklinian Basin strata: insights into the nature of Crockerland and the timing of accretion, Canadian Arctic Islands: Canadian Journal of Earth Sciences, v. 49, p. 1316–1328, https://doi.org/10.1139/e2012-067.

Atwater, T., 1989, Plate tectonic history of the northeast Pacific and western North America, *in* Winterer, E.L., Hussong, D.M., and Decker, R.W., eds., The Eastern Pacific Ocean and Hawaii: Boulder, Colorado, Geological Society of America, Geology of North America, v. N, p. 21–72, https://doi.org/10.1130/DNAG-GNA-N.21.

Bain, H.A., and Hubbard, S.M., 2016, Stratigraphic evolution of a long-lived submarine channel system in the Late Cretaceous Nanaimo Group, British Columbia, Canada: Sedimentary Geology, v. 337, p. 113–132, https://doi.org/10.1016/j.sedgeo.2016.03.010.

Bassett, D., Sutherland, R., Henrys, S., Stern, T., Scherwath, M., Benson, A., Toulmin, S., and Henderson, M., 2010, Three-dimensional velocity structure of the northern Hikurangi margin, Raukumara, New Zealand: Implications for the growth of continental crust by subduction erosion and tectonic underplating: Geochemistry Geophysics Geosystems, v. 11, https://doi.org/10.1029/2010GC003137.

Beck, M.E., 1991, Coastwise transport reconsidered: lateral displacement in oblique subduction zones, and tectonic consequences: Physics of the Earth and Planetary Interiors, v. 68, p. 1–8, https://doi.org/10.1016/0031-9201(91)90002-Y.

Beranek, L.P., McClelland, W.C., van Staal, C.R., Israel, S., and Gordee, S.M., 2017, Late Jurassic flare-up of the Coast Mountains arc systems, NW Canada, and dynamic linkages across the northern Cordillera orogen: Tectonics, v. 36, p. 877–901, https://doi.org/10.1002/2016TC004254.

Brandon, M.T., Orchard, M.J., Parrish, R.R., Sutherland, B.A., and Yorath, C.J., 1986, Fossil ages and isotopic dates from the Paleozoic Sicker Group and associated intrusive rocks, Vancouver Island, British Columbia: Current Research, Part A, Geologic Survey of Canada, Paper 86-1A, p. 683–696.

Brandon, M.T., Cowan, D.S., and Vance, J.A., 1988, The Late Cretaceous San Juan thrust system, San Juan Islands, Washington: Geological Society of America Special Paper 221, 81 p., https://doi.org/10.1130/SPE221-p1.

Brown, E.H., 2012, Obducted nappe sequence in the San Juan Islands–northwest Cascade thrust system, Washington and British Columbia: Canadian Journal of Earth Sciences, v. 49, p. 796–817, https://doi.org/10.1139/e2012-026.

Brown, E.H., and Gehrels, G.E., 2007, Detrital zircon constraints on terrane ages and affinities and timing of orogenic events in the San Juan Islands and North Cascades, Washington: Canadian Journal of Earth Sciences, v. 44, p. 1375–1396, https://doi.org/10.1139/e07-040.

Brown, E.H., Lapen, T.J., Leckie, R.M., Silva, I.P., Verga, D., and Singer, B.S., 2005, Revised ages of blueschist metamorphism and the youngest pre-thrusting rocks in the San Juan Islands, Washington: Canadian Journal of Earth Sciences, v. 42, p. 1389–1400, https://doi.org/10.1139/e05-033.

Brown, E.H., Gehrels, G.E., and Valencia, V.A., 2010, Chilliwack composite terrane in northwest Washington: Neoproterozoic-Silurian passive margin basement, Ordovician-Silurian arc inception: Canadian Journal of Earth Sciences, v. 47, p. 1347–1366, https://doi.org/10.1139/E10-047.

Busby, C., 2004, Continental growth at convergent margins facing large ocean basins: a case study from Mesozoic convergent-margin basins of Baja California, Mexico: Tectonophysics, v. 392, p. 241–277, https://doi.org/10.1016/j.tecto.2004.04.017.

Canil, D., Johnston, S.T., Laroque, J., Friedman, R., and Heaman, M., 2013, Age, construction, and exhumation of the midcrust of the Jurassic Bonanza Arc, Vancouver Island, Canada: Lithosphere, v. 5, p. 82–91, https://doi.org/10.1130/L225.1.

Carter, E.S., and Haggart, J.W., 2006, Radiolarian biogeography of the Pacific region indicates a mid- to high-latitude (>30°) position for the Insular superterrane since the late Early Jurassic, *in* Haggart, J.W., Enkin, R.J., and Monger, J.W.H., eds., Paleogeography of the North American Cordillera: Evidence For and Against Large-Scale Displacements: Geological Association of Canada Special Paper 46, p. 109–132.

Cecil, M.R., Rusmore, M.E., Gehrels, G.E., Woodsworth, G.J., Stowell, H.H., Yokelson, I.N., Chisom, C., Trautman, M., and Homan, E., 2018, Along-strike variation in the magmatic tempo of the Coast Mountains Batholith, British Columbia, and implications for processes controlling episodicity in arcs: Geochemistry Geophysics Geosystems, v. 19, p. 4274–4289, https://doi.org/10.1029/2018GC007874.

Clapp, C.H., 1914, Geology of the Nanaimo map-area: Geological Survey of Canada, Memoir 51, 135 p., https://doi.org/10.4095/101549.

Coutts, D.S., Matthews, W.A., and Hubbard, S.M., 2019, Assessment of widely used methods to derive depositional ages from detrital zircon populations: Geoscience Frontiers, v. 10, p. 1421–1435, https://doi.org/10.1016/j.gsf.2018.11.002.

Cowan, D.S., Brandon, M.T., and Garver, J.I., 1997, Geologic test of hypotheses for large coastwise displacements—a critique illustrated by the Baja British Columbia controversy: American Journal of Science, v. 297, p. 117–173, https://doi.org/10.2475/ajs.297.2.117.

DeBari, S.M., Anderson, R.G., and Mortensen, J.K., 1999, Correlation among lower to upper crustal components in an island arc: the Jurassic Bonanza arc, Vancouver Island, Canada: Canadian Journal of Earth Sciences, v. 36, p. 1371–1413, https://doi.org/10.1139/e99-029.

Dickinson, W.R., 1976, Sedimentary basins developed during evolution of Mesozoic-Cenozoic arc-trench system in western North America: Canadian Journal of Earth Sciences, v. 13, p. 1268–1287, https://doi.org/10.1139/e76-129.

Dickinson, W.R., 1982, Composition of sandstones in circum-Pacific subduction complexes and fore-arc basins: AAPG Bulletin, v. 66, p. 121–137.

Dickinson, W.R., and Gehrels, G.E., 2009, Use of U-Pb ages of detrital zircons to infer maximum depositional ages of strata: a test against a Colorado Plateau Mesozoic database: Earth and Planetary Science Letters, v. 288, p. 115–125, https://doi.org/10.1016/j.epsl.2009.09.013.

Dickinson, W.R., Beard, S.L., Brakenridge, G.R., Erjavec, J.L., Ferguson, R.C., Inman, K.F., Knepp, R.A., Lindberg, F.A., and Ryberg, P.L., 1983, Provenance of North American Phanerozoic sandstones in relation to tectonic setting: Geological Society of America Bulletin, v. 94, p. 222–235, https://doi.org/10.1130/0016-7606(1983)94<222:PONAPS>2.0.CO;2.

Doubrovine, P.V., and Tarduno, J.A., 2008, A revised kinematic model for the relative motion between Pacific oceanic plates and North America since the Late Cretaceous: Journal of Geophysical Research, v. 113, https://doi.org/10.1029/2008JB005585.

Ducea, M.N., and Chapman, A.D., 2018, Sub-magmatic arc underplating by the trench and forearc materials in shallow subduction systems: a geologic perspective and implications: Earth-Science Reviews, v. 185, p. 763–779, https://doi.org/10.1016/j.earscirev.2018.08.001.

Dumitru, T.A., Elder, W.P., Hourigan, J.K., Chapman, A.D., Graham, S.A., and Wakabayashi, J., 2016, Four Cordilleran paleorivers that connected Sevier thrust zones in Idaho to depocenters in California, Washington, Wyoming, and, indirectly, Alaska: Geology, v. 44, p. 75–78, https://doi.org/10.1130/G37286.1.

Eddy, M.P., Clark, K.P., and Polenz, M., 2017, Age and volcanic stratigraphy of the Eocene Siletzia oceanic plateau in Washington and on Vancouver Island: Lithosphere, v. 9, p. 652–664, https://doi.org/10.1130/L650.1.

Encinas, A., Finger, K.L., Buatois, L.A., and Peterson, D.E., 2012, Major forearc subsidence and deep-marine Miocene sedimentation in the present Coastal Cordillera and Longitudinal Depression of south-central Chile (38°30′S-41°45′S): Geological Society of America Bulletin, v. 124, p. 1262–1277, https://doi.org/10.1130/B30567.1.

Engebretson, D.C., Cox, A., and Gordon, R.G., 1985, Relative Motions between Oceanic and Continental Plates in the Pacific Basin: Geological Society of America Special Paper 206, 59 p., https://doi.org/10.1130/SPE206-p1.

England, T.D.J., 1990, Late Cretaceous to Paleogene structural evolution of the Georgia Basin, southwestern British Columbia [Ph.D. thesis]: St John's, Newfoundland, Canada, Memorial University.

England, T.D.J., and Hiscott, R.N., 1992, Lithostratigraphy and deep-water setting of the upper Nanaimo Group (Upper Cretaceous), outer Gulf Islands of southwestern British Columbia: Canadian Journal of Earth Sciences, v. 29, p. 574–595, https://doi.org/10.1139/e92-050.

Englert, R.G., Hubbard, S.M., Coutts, D.S., and Matthews, W.A., 2018, Tectonically controlled initiation of contemporaneous deep-water channel systems along a Late Cretaceous continental margin, western British Columbia, Canada: Sedimentology, v. 65, p. 2404–2438, https://doi.org/10.1111/sed.12472.

Englert, R.G., Hubbard, S.M., Matthews, W.A., Coutts, D.S., and Covault, J., 2019, The evolution of submarine slope channel systems: Timing of incision, bypass, and aggradation in Late Cretaceous Nanaimo Group channel-system strata, BC, Canada: Geosphere, v. 16, https://doi.org/10.1130/GES02091.1.

Enkin, R.J., Baker, J., and Mustard, P.S., 2001, Paleomagnetism of the Upper Cretaceous Nanaimo Group, southwestern Canadian Cordillera: Canadian Journal of Earth Sciences, v. 38, p. 1403–1422, https://doi.org/10.1139/e01-031.

Fairchild, L.H., and Cowan, D.S., 1982, Structure, petrology, and tectonic history of the Leech River complex northwest of Victoria, Vancouver Island: Canadian Journal of Earth Sciences, v. 19, p. 1817–1835, https://doi.org/10.1139/e82-161.

Fedo, C.E., Sircombe, K.N., and Rainbird, R.H., 2003, Detrital zircon analysis of the sedimentary record: Reviews in Mineralogy and Geochemistry, v. 53, p. 277–303, https://doi.org/10.2113/0530277.

Fildani, A., Hessler, A.M., and Graham, S.A., 2008, Trench-forearc interactions reflected in the sedimentary fill of Talara basin, northwest Peru: Basin Research, v. 20, p. 305–331, https://doi.org/10.1111/j.1365-2117.2007.00346.x.

Fitz-Díaz, E., Lawton, T.F., Juarez-Arriaga, E., and Chavez-Cabello, G., 2018, The Cretaceous-Paleogene Mexican orogen: structure, basin development, magmatism and tectonics: Earth-Science Reviews, v. 183, p. 56–84, https://doi.org/10.1016/j.earscirev.2017.03.002.

Friedman, R.M., and Armstrong, R.L., 1995, Jurassic and Cretaceous geochronology of the southern Coast Belt, British, 49° to 51° N, *in* Miller, D.M., and Busby, C., eds., Jurassic Magmatism and Tectonics of the North American Cordillera: Geological Society of America Special Paper 299, p. 95–139, https://doi.org/10.1130/SPE299-p95.

Garver, J., 1988, Stratigraphy, depositional setting, and tectonic significance of the clastic cover to the Fidalgo Ophiolite, San Juan Islands, Washington: Canadian Journal of Earth Sciences, v. 25, p. 417–432, https://doi.org/10.1139/e88-043.

Gehrels, G.E., Valencia, V.A., and Ruiz, J., 2008, Enhanced precision, accuracy, efficiency, and spatial resolution of U-Pb ages by laser ablation–multicollector–inductively coupled

plasma-mass spectrometry: Geochemistry Geophysics Geosystems, v. 9, https://doi.org/10.1029/2007GC001805.

Gehrels, G.E., Rusmore, M., Woodsworth, G., Crawford, M., Andronicos, C., Hollister, L., Patchett, J., Ducea, M., Butler, R., Klepeis, K., Davidson, C., Friedman, R., Haggart, J., Mahoney, B., Crawford, W., Pearson, D., and Girardi, J., 2009, U-Th-Pb geochronology of the Coast Mountains batholith in the north-coastal British Columbia: constraints on age and tectonic evolution: Geological Society of America Bulletin, v. 121, p. 1341–1361, https://doi.org/10.1130/B26404.1.

Goodge, J.W., and Vervoort, J.D., 2006, Origin of Mesoproterozoic A-type granites in Laurentia: Hf isotope evidence: Earth and Planetary Science Letters, v. 243, p. 711–731, https://doi.org/10.1016/j.epsl.2006.01.040.

Greene, A.R., Scoates, J.S., Weis, D., Katvala, E.C., Israel, S., and Nixon, G.T., 2010, The architecture of oceanic plateaus revealed by the volcanic stratigraphy of the accreted Wrangellia oceanic plateau: Geosphere, v. 6, p. 47–73, https://doi.org/10.1130/GES00212.1.

Hadlari, T., Swindles, G.T., Galloway, J.M., Bell, K.M., Sulphur, K.C., Heaman, L.M., Beranek, L.P., and Fallas, K.M., 2015, 1.8 billion years of detrital zircon recycling calibrates refectory part of Earth's sedimentary cycle: PLoS One, v. 10, https://doi.org/10.1371/journal.pone.0144727.

Haggart, J.W., Ward, P.D., and Orr, W., 2005, Turonian (Upper Cretaceous) lithostratigraphy and biochronology, southern Gulf Islands, British Columbia, and northern San Juan Islands, Washington State: Canadian Journal of Earth Sciences, v. 42, p. 2001–2020, https://doi.org/10.1139/e05-066.

Horstwood, M.S.A., Kosler, J.A., Gehrels, G.E., Jackson, S.E., McLean, N.M., Paton, C., Pearson, N.J., Sircombe, K.S., Sylvester, P., Vermeesch, P., Bowring, J.F., Condon, D.J., and Schoene, B., 2016, Community-derived standards for LA-ICP-MS U-(Th-)Pb geochronology—uncertainty propagation, age interpretation and data reporting: Geostandards and Geoanalytical Research, v. 40, p. 311–332, https://doi.org/10.1111/j.1751-908X.2016.00379.x.

Horton, B.K., 2018, Sedimentary record of Andean mountain building: Earth-Science Reviews, v. 178, p. 279–309, https://doi.org/10.1016/j.earscirev.2017.11.025.

Housen, B.A., and Beck, M.E., 1999, Testing terrane transport: an inclusive approach to the Baja B.C. controversy: Geology, v. 27, p. 1143–1146, https://doi.org/10.1130/0091-7613(1999)027<1143:TTTAIA>2.3.CO;2.

Huang, C., Dashtgard, S.E., Kent, B.A.P., Gibson, H.D., and Matthews, W.A., 2019, Resolving the architecture and early evolution of a forearc basin (Georgia Basin, Canada) using detrital zircon: Scientific Reports, v. 9, p. 1–12, https://doi.org/10.1038/s41598-019-51795-5.

Ingersoll, R.V., 1978, Petrofacies and petrologic evolution of the Late Cretaceous fore-arc basin, northern and central California: The Journal of Geology, v. 86, p. 335–352, https://doi.org/10.1086/649695.

Jacobson, C.E., Grove, M., Pedrick, J.N., Barth, A.P., Marsaglia, K.M., Gehrels, G.E., and Nourse, J.A., 2011, Late Cretaceous–early Cenozoic tectonic evolution of the southern California margin inferred from provenance of trench and forearc sediments: Geological Society of America Bulletin, v. 123, p. 485–506, https://doi.org/10.1130/B30238.1.

Johnson, S.Y., Zimmermann, R.A., Naeser, C.W., and Whetten, J.T., 1986, Fission-track dating of the tectonic development of the San Juan Islands, Washington: Canadian Journal of Earth Sciences, v. 23, p. 1318–1330, https://doi.org/10.1139/e86-127.

Johnstone, P.D., Mustard, P.S., and MacEachern, J.A., 2006, The basal unconformity of the Nanaimo Group, southwestern British Columbia: a Late Cretaceous storm-swept rocky shoreline: Canadian Journal of Earth Sciences, v. 43, p. 1165–1181, https://doi.org/10.1139/e06-046.

Jones, M.T., Dashtgard, S.E., and MacEachern, J.A., 2018, A conceptual model for the preservation of thick, transgressive shoreline successions: examples from the forearc Nanaimo basin, British Columbia, Canada: Journal of Sedimentary Research, v. 88, p. 811–826, https://doi.org/10.2110/jsr.2018.40.

Journeay, J.M., and Friedman, R.M., 1993, The Coast Belt thrust system: evidence of Late Cretaceous shortening in southwest British Columbia: Tectonics, v. 12, p. 756–775, https://doi.org/10.1029/92TC02773.

Katnick, D.C., and Mustard, P.S., 2003, Geology of Denman and Hornby islands, British Columbia: implications for Nanaimo Basin evolution and formal definition of the Geoffrey and Spray formations, Upper Cretaceous Nanaimo Group: Canadian Journal of Earth Sciences, v. 40, p. 375–393, https://doi.org/10.1139/e03-005.

Kent, B.A.P., Dashtgard, S.E., Huang, C., MacEachern, J.A., Gibson, H.A., and Cathyl-Huhn, G., 2019, Initiation and early evolution of a forearc basin: Georgia Basin, Canada: Basin Research, https://doi.org/10.1111/bre.12378.

Kimbrough, D.L., Smith, D.P., Mahoney, J.B., Moore, T.E., Grove, M., Gastil, R.G., and Ortega-Rivera, A., 2001, Forearc-basin sedimentary response to rapid Late Cretaceous batholith emplacement in the Peninsular Ranges of southern and Baja California: Geology, v. 29, p. 491–494, https://doi.org/10.1130/0091-7613(2001)029<0491:FBSRTR>2.0.CO;2.

Kley, J., Monaldi, C.R., and Salfity, J.A., 1999, Along-strike segmentation of the Andean foreland: causes and consequences: Tectonophysics, v. 301, p. 75–94, https://doi.org/10.1016/S0040-1951(98)90223-2.

LaMaskin, T.A., 2012, Detrital zircon facies of Cordilleran terranes in western North America: GSA Today, v. 22, p. 4–11, https://doi.org/10.1130/GSATG142A.1.

Ludwig, K.R., 2012, Isoplot v. 3.75—A geochronological Toolkit for Microsoft Excel: Berkeley Geochronology Center, Special Publication, v. 5, p. 1–75.

Mahoney, J.B., Mustard, P.S., Haggart, J.W., Frideman, R.M., Fanning, M.C., and McNicoll, V.J., 1999, Archean zircons in the Cretaceous strata of the western Canadian Cordillera: The "Baja B.C." hypothesis fails a "crucial test": Geology, v. 27, p. 195–198, https://doi.org/10.1130/0091-7613(1999)027<0195:AZICSO>2.3.CO;2.

Malatesta, C., Gerya, T., Crispini, L., Federico, L., and Capponi, G., 2013, Oblique subduction modelling indicates along-trench tectonic transport of sediments: Nature Communications, v. 4, p. 2456, https://doi.org/10.1038/ncomms3456.

Malatesta, C., Gerya, T., Crispini, L., Federico, L., and Capponi, G., 2016, Interplate deformation at early-stage oblique subduction: 3-D thermomechanical numerical modeling: Tectonics, v. 35, p. 1610–1625, https://doi.org/10.1002/2016TC004139.

Matthews, W.A., and Guest, B., 2017, A practical approach for collecting large-*n* detrital zircon U-Pb data sets by quadrupole LA-ICP-MS: Geostandards and Geoanalytical Research, v. 41, p. 161–180, https://doi.org/10.1111/ggr.12146.

Matthews, W.A., Guest, B., Coutts, D.S., Bain, H., and Hubbard, S., 2017, Detrital zircons from the Nanaimo basin, Vancouver Island, British Columbia: An independent test of the Late Cretaceous to Cenozoic northward translation: Tectonics, v. 36, p. 854–876, https://doi.org/10.1002/2017TC004531.

Matzel, J.E.P., Bowring, S.A., and Miller, R.B., 2004, Protolith age of the Swakane Gneiss, North Cascades, Washington: Evidence of rapid underthrusting of sediments beneath an arc: Tectonics, v. 23, https://doi.org/10.1029/2003TC001577.

McGroder, M.F., 1989, Structural geology and kinematic evolution of the eastern Cascade foldbelt, Washington and British Columbia: Canadian Journal of Earth Sciences, v. 26, p. 1586–1602, https://doi.org/10.1139/e89-135.

Miller, R.B., Paterson, S.R., and Matzel, J.E.P., 2009, Plutonism at different crustal levels: insights from the ~5–40 km (paleodepth) North Cascades crustal section, Washington, *in* Miller, R.B., and Snoke, A.W., eds., Crustal Cross Sections from the Western North America Cordillera and Elsewhere: Implications for Tectonic and Petrologic Processes: Geologic Society of America Special Paper 456, p. 125–149, https://doi.org/10.1130/2009.2456(05).

Monger, J.W.H., and Gibson, H.D., 2019, Mesozoic-Cenozoic deformation in the Canadian Cordillera: The record of a "Continental bulldozer"?: Tectonophysics, v. 757, p. 153–169, https://doi.org/10.1016/j.tecto.2018.12.023, https://doi.org/10.1016/j.tecto.2018.12.023.

Monger, J.W.H., Price, R.A., and Templeman-Kluit, D.J., 1982, Tectonic accretion and the origin of the two major metamorphic and plutonic welts in the Canadian Cordillera: Geology, v. 10, p. 70–75, https://doi.org/10.1130/0091-7613(1982)10<70:TAATOO>2.0.CO;2.

Moxon, I.W., and Graham, S.A., 1987, History and controls of subsidence in the Late Cretaceous–Tertiary Great Valley forearc basin, California: Geology, v. 15, p. 626–629, https://doi.org/10.1130/0091-7613(1987)15<626:HACOSI>2.0.CO;2.

Muller, J.E., and Jeletzky, J.A., 1970, Geology of the upper Cretaceous Nanaimo Group, Vancouver Island and Gulf Islands, British Columbia: Geological Survey of Canada, Paper 69-25.

Mustard, P.S., 1994, The Upper Cretaceous Nanaimo Group, Georgia Basin, *in* Monger, J.W.H., ed., Geology and geological hazards of the Vancouver Region, Southwestern British Columbia: Geological Survey of Canada Bulletin, v. 481, p. 27–95.

Mustard, P.S., Parrish, R.R., and McNicoll, V., 1995, Provenance of the Upper Cretaceous Nanaimo Group, British Columbia: Evidence from U-Pb analyses of detrital zircons, *in* Dorobek, S.L., and Ross, G.M., eds., Stratigraphic Evolution of Foreland Basins: SEPM Special Publication 52, p. 65–76, https://doi.org/10.2110/pec.95.52.0065.

Orme, D.A., and Laskowski, A.K., 2016, Basin analysis of the Albian-Santonian Xigaze forearc, Lazi region, south-central Tibet: Journal of Sedimentary Research, v. 86, p. 894–913, https://doi.org/10.2110/jsr.2016.59.

Pacht, J.A., 1984, Petrologic evolution and paleogeography of the Late Cretaceous Nanaimo basin, Washington and British Columbia: Implications for Cretaceous tectonics: Geological Society of America Bulletin, v. 95, p. 766–778, https://doi.org/10.1130/0016-7606(1984)95<766:PEAPOT>2.0.CO;2.

Paterson, S.R., and Ducea, M.N., 2015, Arc magmatic tempos: gathering the evidence: Elements, v. 11, p. 91–98, https://doi.org/10.2113/gselements.11.2.91.

Paterson, S.R., Miller, R.B., Alsleben, H., Whitney, D.L., Valley, P.M., and Hurlow, H., 2004, Driving mechanisms for >40 km of exhumation during contraction and extension in a continental arc, Cascade core, Washington: Tectonics, v. 23, https://doi.org/10.1029/2002TC001440.

Pettijohn, F.J., Potter, P.E., and Siever, R., 1972, Sand and Sandstone: Berlin, Springer, 583 p., https://doi.org/10.1007/978-1-4615-9974-6.

Rowe, C.A., Mustard, P.S., Mahoney, J.B., and Katnick, D.C., 2002, Oriented clastic dike swarms as indicators of paleoslope? An example from the Upper Cretaceous Nanaimo Group, Canada: Journal of Sedimentary Research, v. 72, p. 192–200, https://doi.org/10.1306/062201720192.

Rubin, C.M., Saleeby, J.B., Cowan, D.S., Brandon, M.T., and McGroder, M.F., 1990, Regionally extensive mid-Cretaceous west-vergent thrust system in the northwestern Cordillera: implications for continent-margin tectonism: Geology, v. 18, p. 276–280, https://doi.org/10.1130/0091-7613(1990)018<0276:REMCWV>2.3.CO;2.

Rusmore, M.E., and Woodsworth, G.J., 1994, Evolution of the eastern Waddington thrust belt and its relation to mid-Cretaceous Coast Mountains arc, western British Columbia: Tectonics, v. 13, p. 1052–1067, https://doi.org/10.1029/94TC01316.

Saleeby, J., 2003, Segmentation of the Laramide slab—evidence from the southern Sierra Nevada region: Geological Society of America Bulletin, v. 115, p. 655–668, https://doi.org/10.1130/0016-7606(2003)115<0655:SOTLSF>2.0.CO;2.

Sauer, K.B., Gordon, S.M., Miller, R.B., Vervoort, J.D., and Fisher, C.M., 2017, Evolution of the Jura-Cretaceous North American Cordillera margin: Insights from detrital-zircon U-Pb and Hf isotopes of sedimentary units of the North Cascade Range, Washington: Geosphere, v. 13, p. 2094–2118, https://doi.org/10.1130/GES01501.1.

Sauer, K.B., Gordon, S.M., Miller, R.B., Vervoort, J.D., and Fisher, C.M., 2018, Provenance and metamorphism of the Swakane Gneiss: Implications for incorporation of sediment into the deep levels of the North Cascades continental magmatic arc, Washington: Lithosphere, v. 10, p. 460–477, https://doi.org/10.1130/L712.1.

Sauer, K.B., Gordon, S.M., Miller, R.B., Jacobson, C.E., Grove, M.G., Vervoort, J.D., and Fisher, C.M., 2019, Deep-crustal metasedimentary rocks support Late Cretaceous "Mojave-BC" translation: Geology, v. 47, p. 99–102, https://doi.org/10.1130/G45554.1.

Saylor, J.E., Stockli, D.F., Horton, B.K., Nie, J., and Mora, A., 2012, Discriminating rapid exhumation from syndepositional volcanism using detrital zircon double dating: Implications for the tectonic history of the Eastern Cordillera, Colombia: Geological Society of America Bulletin, v. 124, p. 762–779, https://doi.org/10.1130/B30534.1.

Schermer, E.R., Hoffnagle, E.A., Brown, E.H., Gehrels, G.E., and McClelland, W.C., 2018, U-Pb and Hf isotopic evidence for an Arctic origin of terranes in northwestern Washington: Geosphere, v. 14, p. 835–860, https://doi.org/10.1130/GES01557.1.

Schiarizza, P., Gaba, R.G., Coleman, M.E., Gamer, J.I., and Glover, J.K., 1990, Geology and mineral occurrences of the Yalakom River area: British Columbia Ministry of Energy, Mines, and Petroleum Resources, 1989-1, p. 53–72.

Seton, M., Muller, R.D., Zahirovic, S., Gaina, C., Torsvik, T., Shephard, G., Talsma, A., Gurnis, M., Turner, M., Maus, S., and Chandler, M., 2012, Global continental and ocean basin reconstructions since 200 Ma: Earth-Science Reviews, v. 113, p. 212–270, https://doi.org/10.1016/j.earscirev.2012.03.002.

Sharman, G.R., Graham, S.A., Grove, M., Kimbrough, D.L., and Wright, J.E., 2015, Detrital zircon provenance of the Late Cretaceous–Eocene California forearc: Influence of Laramide low-angle subduction on sediment dispersal and paleogeography: Geological Society of America Bulletin, v. 127, p. 38–60, https://doi.org/10.1130/B31065.1.

Sharman, G.R., Sharman, J.P., and Sylvester, Z., 2018, detritalPy: a Python-based toolset for visualizing and analysing detrital geo-thermochronologic data: Depositional Record, v. 4, p. 202–215, https://doi.org/10.1002/dep2.45.

Sigloch, K., and Mihalynuk, M.G., 2017, Mantle and geological evidence for a Late Jurassic–Cretaceous suture spanning North America: Geological Society of America Bulletin, v. 129, p. 1489–1520, https://doi.org/10.1130/B31529.1.

Sluggett, C.L., 2003, Uranium-lead age and geochemical constraints on Paleozoic early Mesozoic magmatism in Wrangellia Terrane, Saltspring Island, British Columbia, Canada [BSc thesis]: Vancouver, British Columbia, University of British Columbia, 84 p.

Spencer, C.S., and Kirkland, C.L., 2016, Visualizing the sedimentary response through the orogenic cycle: A multidimensional scaling approach: Lithosphere, v. 8, p. 29–37, https://doi.org/10.1130/L479.1.

Sundell, K.E., Saylor, J.E., Lapen, T.J., Styron, R.H., Villareal, D., Usnayo, P., and Cardenas, J., 2018, Peruvian Altiplano stratigraphy highlights along-strike variation in foreland basin evolution of the Cenozoic central Andes: Tectonophysics, v. 37, p. 1876–1904.

Surpless, K.D., Sickmann, Z.T., and Koplitz, T.A., 2014, East-derived strata in the Methow basin record rapid mid-Cretaceous uplift of the southern Coast Mountains batholith: Canadian Journal of Earth Sciences, v. 51, p. 339–357, https://doi.org/10.1139/cjes-2013-0144.

Tabor, R.W., Zartman, R.E., and Frizzell, V.A., Jr., 1987, Possible tectonostratigraphic terranes in the North Cascades crystalline core, Washington, *in* Schuster, J.E., ed., Selected papers on the geology of Washington: Washington Division of Geology and Earth Resources Bulletin, v. 77, p. 107–127.

Umhoefer, P.J., 1987, Northward translation of "BAJA British Columbia" along the Late Cretaceous to Paleocene margin of western North America: Tectonics, v. 6, p. 377–394, https://doi.org/10.1029/TC006i004p00377.

Umhoefer, P.J., and Miller, R.N., 1996, Mid-Cretaceous thrusting in the southern Coast Belt, British Columbia and Washington, after strike-slip fault reconstruction: Tectonics, v. 15, p. 545–565, https://doi.org/10.1029/95TC03498.

Valley, P.M., Whitney, D.L., Paterson, S.R., Miller, R.B., and Alsleben, H., 2003, Metamorphism of the deepest exposed arc rocks in the Cretaceous to Paleogene Cascades belt, Washington: evidence for large-scale vertical motion in a continental arc: Journal of Metamorphic Geology, v. 21, p. 203–220, https://doi.org/10.1046/j.1525-1314.2003.00437.x.

Vance, J.A., 1975, Bedrock geology of San Juan County, *in* Russel, R.H., eds., Geology and water resources of the San Juan Islands, San Juan County Washington: Washington Department of Ecology Office of Technical Services Water Supply Bulletin, no. 46, p. 1–39.

Vermeesch, P., 2013, Multi-sample comparison of detrital age distributions: Chemical Geology, v. 341, p. 140–146, https://doi.org/10.1016/j.chemgeo.2013.01.010.

von Huene, R., and Scholl, D.W., 1991, Observations at convergent margins concerning sediment subduction, subduction erosion, and the growth of continental crust: Reviews of Geophysics, v. 29, p. 279–316, https://doi.org/10.1029/91RG00969.

Ward, P.D., Haggart, J.W., Mitchell, R., Kirschvink, J.L., and Tobin, T., 2012, Integration of macrofossil biostratigraphy and magnetostratigraphy for the Pacific Coast Upper Cretaceous (Campanian-Maastrichtian) of North America and implications for correlation with the Western Interior Tethys: Geological Society of America Bulletin, v. 124, p. 957–974, https://doi.org/10.1130/B30077.1.

Whitchurch, A.I., Carter, A., Sinclair, H.D., Duller, R.A., Whittaker, A.C., and Allen, P.A., 2011, Sediment routing systems evolution within a diachronously orogen: Insights from detrital zircon thermochronological analyses from the South-central Pyrenees: American Journal of Science, v. 311, p. 442–482, https://doi.org/10.2475/05.2011.03.

White, C., Gehrels, G.E., Pecha, M., Giesler, D., Yokelson, I., McClelland, W.C., and Butler, R.F., 2016, U-Pb and Hf isotope analysis of detrital zircons from Paleozoic strata of the southern Alexander terrane (southeast Alaska): Lithosphere, v. 8, p. 83–96, https://doi.org/10.1130/L475.1.

Whitmeyer, S.J., and Karlstrom, K.E., 2007, Tectonic model for the Proterozoic of North America: Geosphere, v. 3, p. 220–259, https://doi.org/10.1130/GES00055.1.

Woods, M.T., and Davies, G.F., 1982, Late Cretaceous genesis of the Kula plate: Earth and Planetary Science Letters, v. 58, p. 161–166, https://doi.org/10.1016/0012-821X(82)90191-1.

Wyld, S.J., Umhoefer, P.J., Wright, J.E., Haggart, J.W., Enkin, R.J., and Monger, J.W.H., 2006, Reconstructing northern Cordilleran terranes along known Cretaceous and Cenozoic strike-slip faults: Implications for the Baja British Columbia hypothesis and other models, *in* Haggart, J.W., Enkin, R.J., and Monger, J.W.H., eds., Paleogeography of the North American Cordillera: Evidence For and Against Large-Scale Displacements: Geological Association of Canada Special Paper 46, p. 277–298.

Yin, A., 2006, Cenozoic tectonic evolution of the Himalayan orogen as constrained by along-strike variation of structural geometry, exhumation history, and foreland sedimentation: Earth-Science Reviews, v. 76, p. 1–131, https://doi.org/10.1016/j.earscirev.2005.05.004.

Yonkee, W.A., and Weil, A.B., 2015, Tectonic evolution of the Sevier and Laramide belts within the North American Cordillera orogenic system: Earth-Science Reviews, v. 150, p. 531–593, https://doi.org/10.1016/j.earscirev.2015.08.001.

Yorath, C.J., Sutherland Brown, A., and Massey, N.W.D., 1999, LITHOPROBE, southern Vancouver Island, British Columbia: Geological Survey of Canada Bulletin, v. 498, 145 p., https://doi.org/10.4095/210350.

MANUSCRIPT RECEIVED 29 AUGUST 2019
REVISED MANUSCRIPT RECEIVED 20 NOVEMBER 2019
MANUSCRIPT ACCEPTED 4 FEBRUARY 2020